A Kinematic-Coupling-Based Adaptive Fixture for High Precision Positioning Applications in Flexible Manufacturing Systems

by

Carlos A. Araque

B.S. Mechanical Engineering
Massachusetts Institute of Technology, 2001

Submitted to the Department of Mechanical Engineering in Partial Fulfillment of the Requirements for the Degree of Master of Science in Mechanical Engineering

at the

Massachusetts Institute of Technology

September 2002

Signature of Author ----------
Department of Mechanical Engineering
August 9, 2002

Certified by ----------
Martin L. Culpepper
Assistant Professor of Mechanical Engineering
Thesis Supervisor

Accepted by ---------- ----------
Ain A. Sonin
Chairman, Department Committee on Graduate Students

A Kinematic-Coupling-Based Adaptive Fixture for High Precision Positioning Applications in Flexible Manufacturing Systems

by

CARLOS A. ARAQUE

Submitted to the Department of Mechanical Engineering on August 9, 2002 in Partial Fulfillment of the Requirements for the Degree of Master of Science in Mechanical Engineering

ABSTRACT

The means to achieve micron level accuracy and repeatability with detachable fixtures will be an enabling technology in future manufacturing processes. Given the many sources of time variable errors in fixture alignment (i.e. thermal, load, vibration), the integration of actuators and sensors within fixtures will be necessary to achieve real-time error compensation. This thesis examines the fundamental issues and design challenges associated with implementing a first prototype of a mechanized fixture. The device utilizes adjustable parallel kinematics (to achieve accuracy) and the interface of a three-groove kinematic coupling (to achieve repeatability). The result is a new fixture technology, dubbed the Accurate and Repeatable Kinematic Coupling (ARKC).

The ARKC is equipped to accept six independent actuation inputs that make it possible to obtain decoupled small-motion adjustment in six axes. The kinematic model for the adjustable position control of the coupling is derived. The main contribution of this thesis is the experimental verification of the model. Experiments show less than 13% systematic error between the adjustable kinematic theory and experimental data. Although not a subject of this work, the systematic error can be mapped and removed from the coupling performance via software. The result will be a coupling with accuracy and repeatability of approximately 5 microns.

Implementation of the device in flexible manufacturing systems is discussed. A case study that examines the performance of the ARKC in a next generation manufacturing process is included. Theoretical results from the case study show that the ARKC can be used to provide the precision alignment and positioning requirements of next generation semiconductor test equipment.

Thesis Supervisor: Martin L. Culpepper

Title: Assistant Professor of Mechanical Engineering

ACKNOWLEDGMENTS

The completion of this thesis sets an important milestone in my career as a Mechanical Engineer. I want to acknowledge the many who helped me along the way.

I want to thank God.

I want to thank my precious Tina. Her constant support helped me endure the endless hours of work and inspired me to do my very best.

I want to thank my little Alejandro who fills my life with joy with every single step he takes in growing up.

I want to thank my family for helping me realize my full potential.

I want to thank my advisor, Professor Martin L. Culpepper, for the many hours he dedicated to the completion of this project and for encouraging me to create and pursue my own goals.

And finally, I want to thank my colleagues and friends, Gordon, Patrick, and Marcos, for providing valuable insight.

TABLE OF CONTENTS

LIST OF FIGURES

LIST OF TABLES

Chapter 1

INTRODUCTION

1.1 Motivation

There is a clear trend in industry toward more efficient and precise manufacturing processes. This is motivated by the need to create higher quality products. The manufacture of these products depends on the ability of manufacturing operations to accurately and repeatably align and maintain the position of objects. This has been achieved in a number of different ways with positioning methods that rely on elastic averaging principles, kinematic principles or a combination of both [1]. Elastic averaging positioning methods are good for applications with high loads and kinematic methods are well suited for applications that require moderate stiffness and repeatability better than 5μm.

In addition to high repeatability, manufacturers are increasingly requiring the automation of these positioning methods in order to incorporate them into flexible manufacturing systems (FMS). Low-cost static devices (i.e. devices that remain fixed after their initial setup) are widely used for fixturing operations. Although these devices have proven to be cost-effective in automated manufacturing operations, their initial setup and calibration takes a significant amount of time and thus reduces the productivity and constrains the flexibility of flexible manufacturing systems. On the other hand, active positioning devices (i.e. devices that can change part to part location at any time) can offer improved

flexibility because their calibration and initial setup can be automated. In addition, they can be reconfigured quickly to operate in a number of different processes by simply uploading a different set of instructions to them. The downside to these devices is their elevated cost which can range in the tens of thousands of dollars when accuracy and repeatability better than 5μm are necessary. Maintenance costs add a significant amount to the total cost of operation of these devices, especially when they must withstand harsh environmental conditions.

In order to address these problems (e.g. reduce setup and calibration time via automation, decrease cost of operation while maintaining good accuracy and repeatability), the Precision System Design and Manufacturing (PSDAM) lab at MIT has developed the Adjustable and Repeatable Kinematic Coupling (ARKC). The ARKC is a kinematic coupling in which each of the three balls is equipped with a dual motion (linear and rotary) actuator. In this way, the ARKC provides fast, accurate and repeatable positioning in 6 axes (3 balls x 2 independent motions = 6 axes). This is a desirable characteristic in the manufacturing, assembly and testing of precision parts.

This thesis presents the theoretical foundation to design the ARKC. It compliments the experimental study completed by Rodríguez in "Design and Manufacturing of an ARKC" [2]. Rodríguez's study presents the practical considerations to design and manufacture the ARKC with emphasis on the materials and processes used to create it, the geometry of the coupling and the actuators needed to position the coupling in six axes.

1.2 Thesis Scope and Organization

1.2.1 Scope

This thesis examines the theory used to model and analyze the adjustable kinematics of the ARKC in six axes. The theory is combined with existing kinematic coupling theory and used to quantify the accuracy, repeatability, stiffness and error budget of the coupling based on design parameters. A case study is presented to illustrate implementation of the ARKC concept in semiconductor test equipment.

The thesis also covers the background needed to understand two important industrial communication networks: DeviceNet and Foundation Fieldbus. These networks are widely used in industry as a mean to control and transmit information between devices and machines that make up flexible manufacturing systems. These networks are examined in the context of the ARKC in automated manufacturing operations. The ways in which the ARKC benefits from these communication networks is also discussed.

1.2.2 Organization and Content

The first chapter of this thesis discusses the importance of the research on adjustable and repeatable fixtures. The chapter revolves around four fundamental issues that must be addressed to meet the needs of these fixtures.

The second chapter continues with an overview of the functional requirements of fixtures and examples of common passive and active fixtures used to meet these requirements. The ARKC geometry and function are then presented followed by a discussion of how the ARKC addresses the fundamental issues outlined in the first chapter. The chapter ends with coverage of the adjustable kinematic model of the ARKC as developed by Culpepper [3].

The third chapter covers the implementation of an ARKC in flexible manufacturing systems. The chapter starts with an overview of two widely used industrial communication networks and explains how these networks add to the functionality of the ARKC and allow it to be implemented as a modular component of an automated manufacturing operation. The chapter then closes by illustrating the implementation of the ARKC in a manufacturing application.

The performance of the ARKC with respect to the functional requirements of fixtures is presented in the fourth chapter. The metrics for performance are repeatability, accuracy and stiffness. Formulas for estimating the value of these metrics as well as the error budget of the ARKC are also presented in the chapter. The chapter finishes with a

discussion of the effect of component selection on the performance of the ARKC and general guidelines for achieving various levels of performance.

The fifth chapter is a case study on ARKC fixturing in semiconductor test equipment. This chapter illustrates the use of the ARKC concept to reduce the calibration and setup time of test-head docking systems. The thesis ends with a summary of the contributions of this research and a discussion of topics for further investigation.

1.3 Fundamental Issues Addressed by this Thesis

Most of the research in precision fixtures has focused on improving the repeatability and increasing the flexibility of fixtures to accommodate parts with similar features. However, beyond specifying tighter feature size/position tolerances in fixtures, little has been done to improve their accuracy. Static fixture accuracy is a function of manufacture and assembly and remains fixed once the fixture is constructed. For that reason, it is important to provide some means of adjustability. This not only enables accuracy but also active error compensation during manufacturing.

This section examines the needs of next generation fixtures and develops the fundamental issues that must be addressed to meet these needs. The first need is related to repeatability and accuracy. Next generation fixtures will have to be both repeatable and accurate to address the needs of next generation manufacturing processes. The repeatability of fixtures has surpassed micron-level performance but accuracy can be orders of magnitude larger, especially for high performance kinematic fixtures such as kinematic couplings. It is therefore necessary to narrow the gap between a coupling's repeatability and accuracy. In addition, it is desirable that the fixture be automated to ensure its proper integration into automated manufacturing operations. The fundamental issue that must be addressed to satisfy this need can be captured within the following question: How to provide automated micron-level repeatability AND accuracy in precision couplings?

The second need is related to manufacturing yield. The manufacture of high precision components requires reliable positioning methods. Positioning a component with micron-

level precision can be a time-consuming task. Next generation fixtures will have to be able to position components precisely and efficiently to contribute to the overall efficiency of next generation manufacturing processes. The fundamental issue is again contained within the question: How to improve manufacturing yield by in-process optimization of fixturing performance?

The third need is related to active error correction. A fixture can be repeatable and accurate but its performance can be degraded by time variable errors caused by environmental conditions (e.g. temperature, vibration) and wear. It is thus necessary to provide a way to compensate for these errors during the life cycle of the fixture. Next generation fixtures will be required to compensate for time variable errors in order to be useful. The fundamental issue is captured in the question: How to provide active error correction to compensate for time variable errors in detachable fixtures?

The fourth need is related to flexibility, i.e. fixtures that can accommodate multiple variations of the same part. Often, this flexibility is achieved by making fixtures modular and detachable. Next generation fixtures will have to provide this level of flexibility as well. The fundamental issue behind this need can be worded in the following way: How to provide precision fixturing with multiple states of assembly?

We start with an overview of fixtures and an explanation of the new concept for an adjustable and repeatable kinematic fixture.

Chapter 2

MECHANICAL FIXTURES AND THE ARKC

2.1 Fixturing Functional Requirements

Mechanical fixtures are used to locate two or more components with respect to each other. The functional requirements depend on the application but some common functional requirements are listed below:

1. Repeatability: repeatability refers to the ability of the fixture to position the fixtured components in the same location every time. The repeatability of a fixture depends on factors such as the stability of the materials used to manufacture it and its design. Exact-constraint fixtures, fixtures that use a number of contact points equal to the number of desired constrained degrees of freedom, achieve the best repeatability among all types of fixtures (usually sub-micron).

2. Accuracy: accuracy refers to the ability of a fixture to position components in a desired location every time. Accuracy is different from repeatability and a fixture can be very repeatable but not accurate. The accuracy of a fixture depends on the manufacturing tolerances and assembly processes employed during its creation.

3. Stiffness: stiffness refers to the ability of a fixture to withstand disturbance forces with minimum displacements. The stiffness of a fixture depends on factors such as the materials used to manufacture it and its design.

2.2 Passive Mechanical Fixtures

Passive fixtures can generally be considered rigid bodies with a specialized function. They are often designed with a particular application in mind and cannot be changed once they have been manufactured. Passive mechanical fixtures may provide some degree of flexibility and are often made to accommodate a whole family of parts with similar features.

2.2.1 Elastically Averaged Fixtures

These fixtures operate according to the principle of elastic averaging. They are called "elastically averaged" because contacting interfaces have many contact points which elastically deform when the fixture is engaged. The location of the components of the fixture depends on an averaging of the elastic deformations of the contact points. These fixtures are non-kinematic, i.e. it is not possible to compute their performance in closed form. These fixtures are useful in applications that require high stiffness, large load bearing capacity and repeatability on the order of 5μm. Figure 2.1 shows two examples of contacting elements used in this type of fixture.

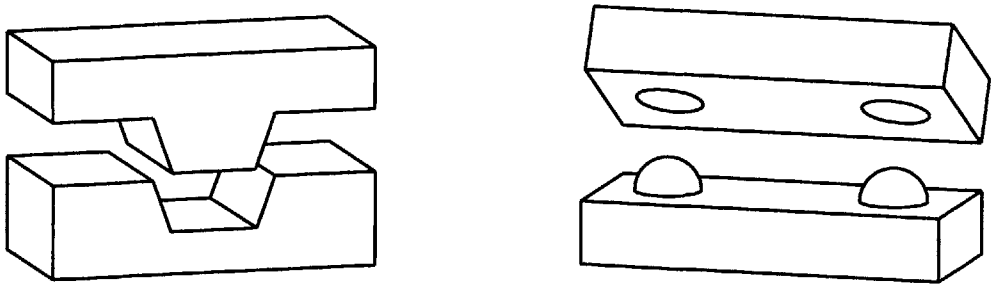

***Figure 2.1** – Examples of contacting elements used in elastically averaged fixtures*

2.2.2 Pinned Joints

Pinned joints consist of a set of aligning pins that mate with a corresponding set of aligning holes or slots as seen in Figure 2.2a. When the clearance between the pins and the slots is identically zero or is negative (i.e. interference), a pinned joint becomes over constrained. On the other hand, if there is a finite clearance between the pins and the slots, the pinned joint results in uncertainty in the relative location of the components to be mated. This is acceptable as long as the degree of uncertainty is below the repeatability required for the joint. A pinned joint has practical repeatability on the order of 5-10μm.

Pinned joints are susceptible to jamming and wedging. Consider for example Figure 2.2b. This figure shows a locating pin as it enters its corresponding slot. If the clearance between the pin and the slot is small compared to their diameter, jamming occurs until the length of engagement between the two increases over a critical value [4]. Jamming and wedging increase assembly time, lower productivity and may result in pinched fingers if assembly is done manually.

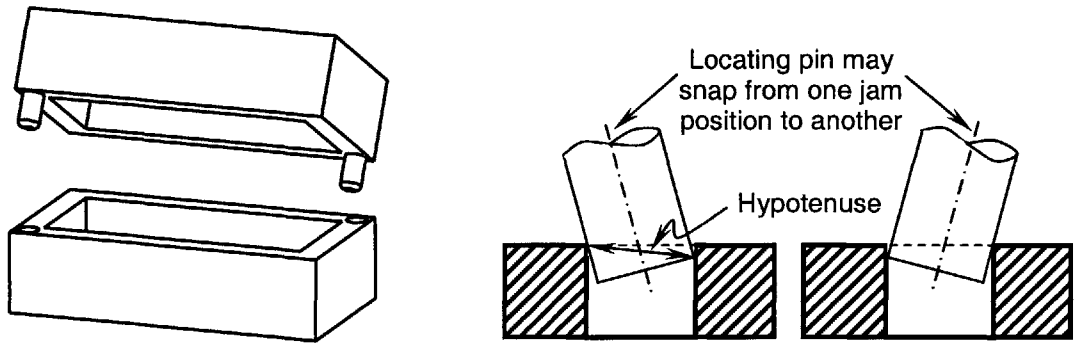

***Figure 2.2** – (a) Example of a pin-hole joint; (b) jamming of a pinned joint*

2.2.3 Kinematic Couplings

Kinematic couplings (Figure 2.3) are deterministic couplings based on exact constraint principles. This means that the number of points of contact between the two halves of the

coupling is equal to the number of degrees of freedom to be constrained. A typical kinematic coupling constrains six degrees of freedom (three translations and three rotations) and thus has six points of contact. They are called kinematic because a closed form solution for the kinematics/location of the two halves of the coupling relative to each other can be derived. The repeatability of a kinematic coupling (sub-micron) can be orders of magnitude better than its accuracy. Accuracy is attained via mechanical adjustments and via tight production tolerances during the manufacture of the coupling. It is important to note recent work on the accuracy of kinematic fixtures. Barraja and Vallance [5] investigate analytic methods to allocate tolerances to dimensions in kinematic couplings in order to optimize their accuracy and minimize their production cost. Though this is a wonderful development for static kinematic couplings, devices such as the ARKC are still needed to provide real-time adjustment and error compensation.

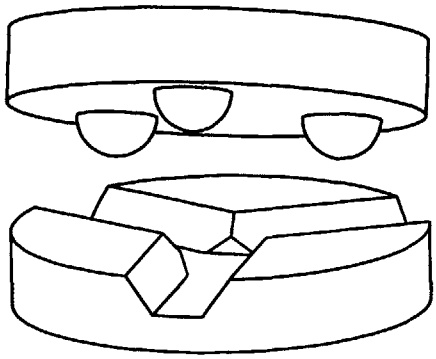

***Figure 2.3** – Conventional three groove kinematic coupling for six degrees of freedom constraint*

2.2.4 Side by Side Comparison of Passive Mechanical Fixtures

Between fixture types, repeatability, accuracy and stiffness can vary widely. These characteristics depend on material selection, fixture design and manufacturing tolerances. The repeatability (practical accuracy for all of them is between 50-100μm) of the three types of passive fixtures discussed above is summarized in Figure 2.4.

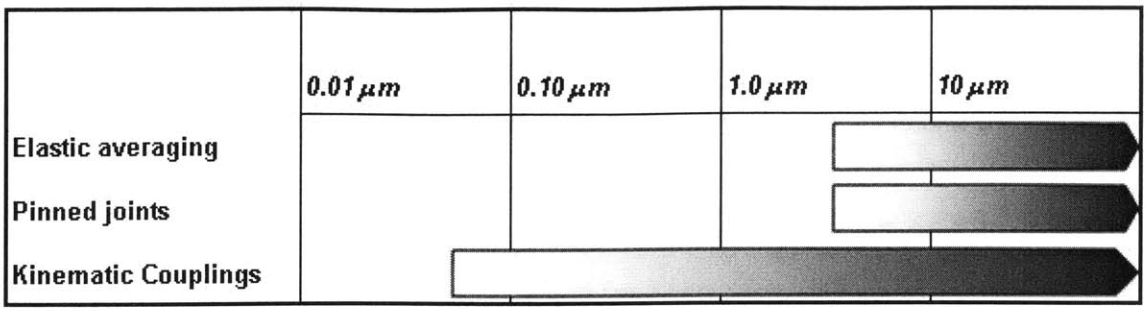

***Figure 2.4** – Side by side repeatability comparison of passive mechanical fixtures (adapted from Culpepper [1])*

2.3 Active Mechanical Fixtures and Positioning Devices

Active fixtures and positioning devices change configuration by means of actuation. This is important as they can be made to automatically calibrate and position themselves for a particular set up. In addition, active fixtures easily adapt to new manufacturing processes by uploading different sets of instructions. They can accurately and repeatably locate components with respect to each other and compensate for errors in real time. These characteristics make them particularly useful in demanding positioning applications. The following sub-sections briefly describe the characteristics of some types of active fixtures. Performance characteristics of each type are reserved until the end of the section where they are compared and summarized in Table 2.1.

2.3.1 Precision X-Y Microstage with Maneuverable Kinematic Coupling Mechanism

This microstage, shown in Figure 2.5, was developed by Taylor and Tu [6]. It consists of a base plate with three v-grooves and a second plate (top plate) with three balls. The first ball is rigidly fixed to the upper plate, and the second and the third balls are maneuverable (with respect to the upper plate) within slots via linear actuators. Actuating the two balls changes the pattern between the three ball centers. The top and bottom components must move relative to each other (balls slide in the grooves) to maintain geometric compatibility at all ball-groove contacts. This movement is deterministic and exploited along with the repeatability of the kinematic coupling to produce a two-

dimensional motion stage. This mechanism has a transmission ratio that provides an increase in positioning resolution over the resolution of the actuators used to control it. The motion of this device can be represented as shown in Figure 2.5.

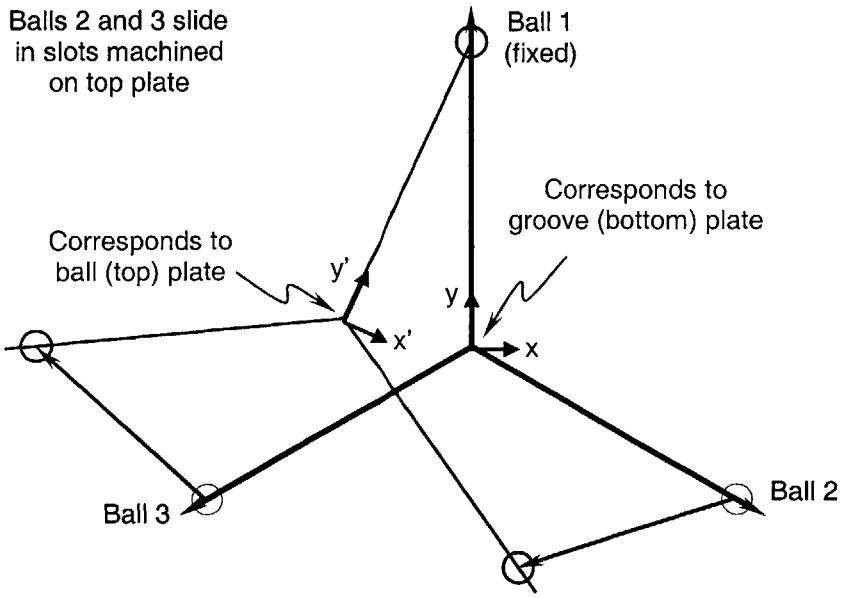

***Figure 2.5** – Precision X-Y microstage with maneuverable kinematic coupling mechanism*

The performance characteristics of the X-Y microstage are shown in Table 2.1 on page 29.

2.3.2 Linear and Rotational Stages

These are composed of linear and/or rotational actuators, guiding bearings and supporting structures. These stages can be arranged in diverse configurations and are often used for testing and inspection procedures because of their high accuracy and repeatability (usually better than 1μm). Individually they have one degree of freedom but can be stacked in series to achieve multi-axis motion. Their cost is around $10K dollars per axis Figure 2.6 shows two examples of these stages. Typical performance characteristics of these stages are shown in Table 2.1 on page 29.

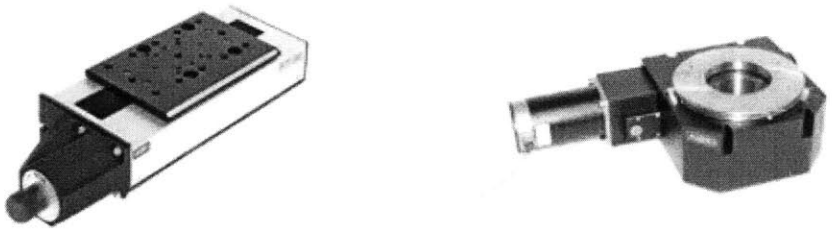

(a) (b)

***Figure 2.6** – (a) Linear and (b) rotational stages (photos courtesy of Phytron, Inc.)*

2.3.3 Stewart-Gough Platforms

Stewart-Gough platforms are composed of six articulated and actuated structural legs arranged to provide six constraints between two components. Figure 2.7 shows an example of a Stewart-Gough platform. Their elevated cost, usually in the order of $30K dollars, is due to part count, tight production tolerances necessary to manufacture them and their increased level of control complexity. Typical performance characteristics of these devices are shown in Table 2.1 on page 29.

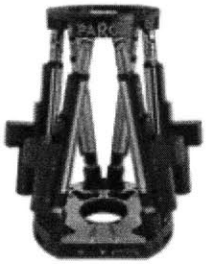

***Figure 2.7** – Stewart-Gough platform (photo courtesy of Phytron, Inc.)*

2.3.4 Adjustable and Repeatable Kinematic Coupling

The adjustable and repeatable kinematic coupling (ARKC) is based on a modified three groove kinematic coupling. Figure 2.8 shows an ARKC. Each ball is constrained so that it has two degrees of freedom with respect to the plate that supports it. These degrees of freedom are controlled by dual motion actuators. In this way the coupling can be

positioned in six degrees of freedom (i.e. two independent motions per ball x three balls). This positioning capability enables compensation for fixturing wear errors and adds flexibility and accuracy to the coupling. The ARKC offers all the advantages of conventional kinematic couplings such as micron-level repeatability, high stiffness and low cost. Typical performance characteristics for the ARKC are shown in Table 2.1 on page 29.

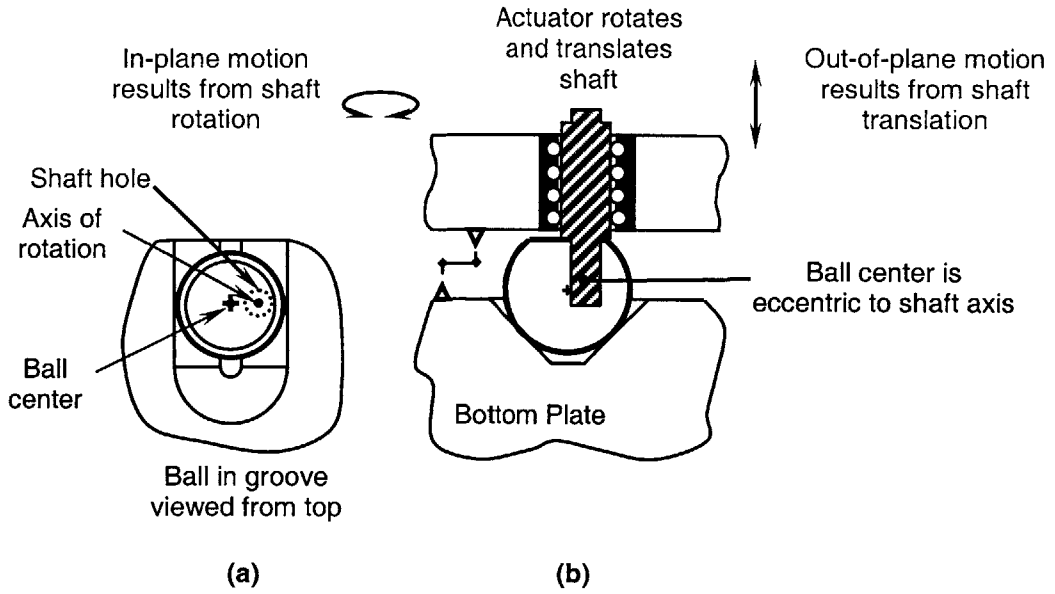

***Figure 2.8** – Adjustable and repeatable kinematic coupling joint concept*

2.3.5 Side by Side Comparison of Active Mechanical Fixtures

The active mechanical fixtures and positioning devices discussed in sections 2.3.1 through 2.3.4 have different performance characteristics. These performance characteristics depend on factors such as the device configuration (e.g. stacked vs. non-stacked configurations for linear stages); the actuators used to control the device (e.g. open-loop stepper motors vs. closed-loop servos for the ARKC); and the operating conditions that the device is designed to withstand (e.g. loads and dynamic forces). Table

2.1 shows typical performance characteristics for these active mechanical fixtures and positioning devices.

Table 2.1 – Performance characteristics of common positioning devices

	Linear Stage	Rotational Stage	S-G Platforms	X-Y Stage	ARKC
Repeatability	< 0.2μm	100μrad	1-2μm 10μrad	< 1μm	< 1μm 10μrad
Accuracy	0.5-10μm	500μrad	1μm 5μrad	1-10μm	1-10μm 20μrad
Resolution	0.001- 0.100μm	10μrad	1μm 5μrad	2μm	< 1μm 10μrad
Range	100mm	360°	500mm 60°	50mm	10mm 5°
Motion	1 axis (stackable)	1 axis (stackable)	6 axes	2 axes	6 axes
Stiffness	100N/μm	1N·m/μrad	100N/μm 1N·m/μrad	150N/μm	150N/μm 20N·m/μrad
Load Capacity	50kg	50kg	100kg	400kg	400kg
Cost [$]	~ 10K	~ 10K	~ 30K	~ 2K	~ 2K

From Table 2.1 we can see that the ARKC has the potential to serve as a low cost alternative to Stewart-Gough platforms and linear and rotational stages. It is capable of providing six axes motion with accuracy and resolution in the order of 1μm without compromising repeatability. The ARKC is examined in greater detail in the rest of the chapter.

2.4 The Adjustable and Repeatable Kinematic Coupling

This section is intended to familiarize the reader with the geometry, modeling and operating principles of the adjustable and repeatable kinematic coupling.

2.4.1 ARKC Geometry and Function

The ARKC enables adjustment in six degrees of freedom by means of six independently actuated axes of control. These axes are illustrated in Figure 2.9. Three of the axes allow the coupling to translate in z and to rotate about the x and y axes. This motion is achieved by moving the balls in the z direction with respect to the top plate as anticipated by Figure 2.8b. The remaining degrees of freedom (x , y and θ_z) are adjusted by rotating the balls around an axis eccentric to the ball center as shown in Figure 2.8a. Selective translation/rotation of the balls allows motion of the coupling in any desired direction.

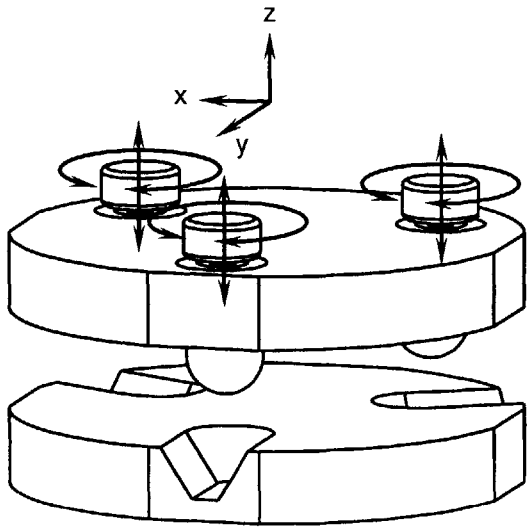

Figure 2.9 – ARKC with six independent axes of control

2.4.2 Mathematical Modeling of the Coupling Motion

In-Plane Motion (x, y, θ_z)

The ARKC accomplishes in-plane motion as shown in Figure 2.10. Figure 2.10a shows the coupling in its home configuration. In this configuration, the vector pointing from the center of a ball to the axis of rotation of the same ball is aligned with the plane of symmetry of the corresponding groove. Figure 2.10b shows a displaced configuration of

the coupling achieved by rotating ball 1 by 90° clockwise, ball 2 by 90° counterclockwise and ball 3 by 180°.

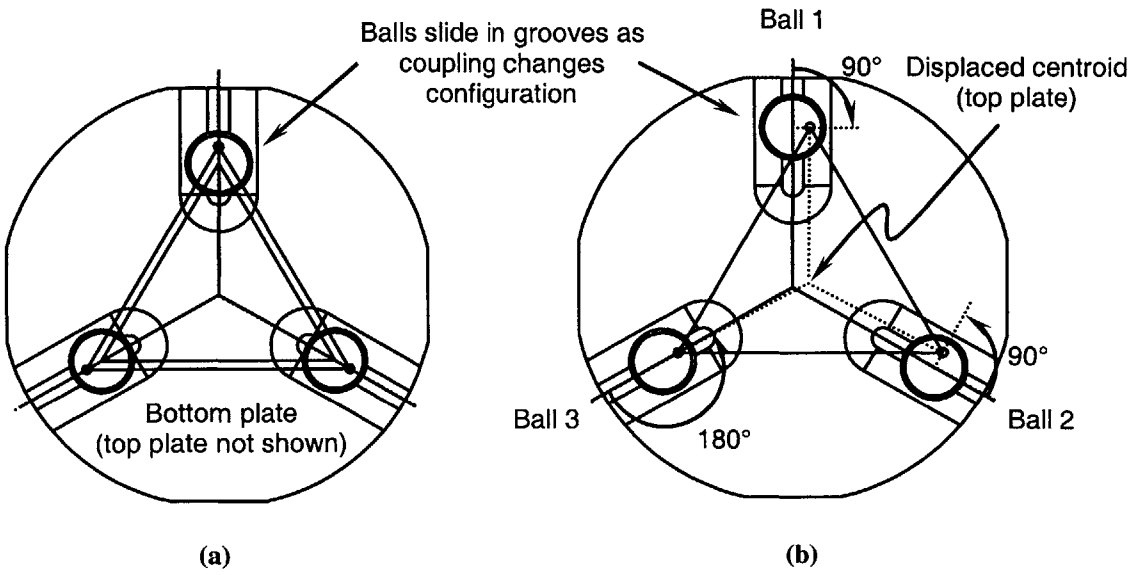

***Figure 2.10** – In-plane motion of the ARKC: (a) home configuration; (b) displaced configuration*

The discussion that follows assumes that the plate containing the grooves, hereafter referred to as the bottom plate, is fixed and its centroid coincides with the origin of a reference coordinate frame. Note that in the home configuration, the centroid of the plate that contains the balls, hereafter referred to as the top plate, coincides with the origin of the reference coordinate frame as well. The configuration shown in Figure 2.10b can be modeled as shown in Figure 2.11 [3].

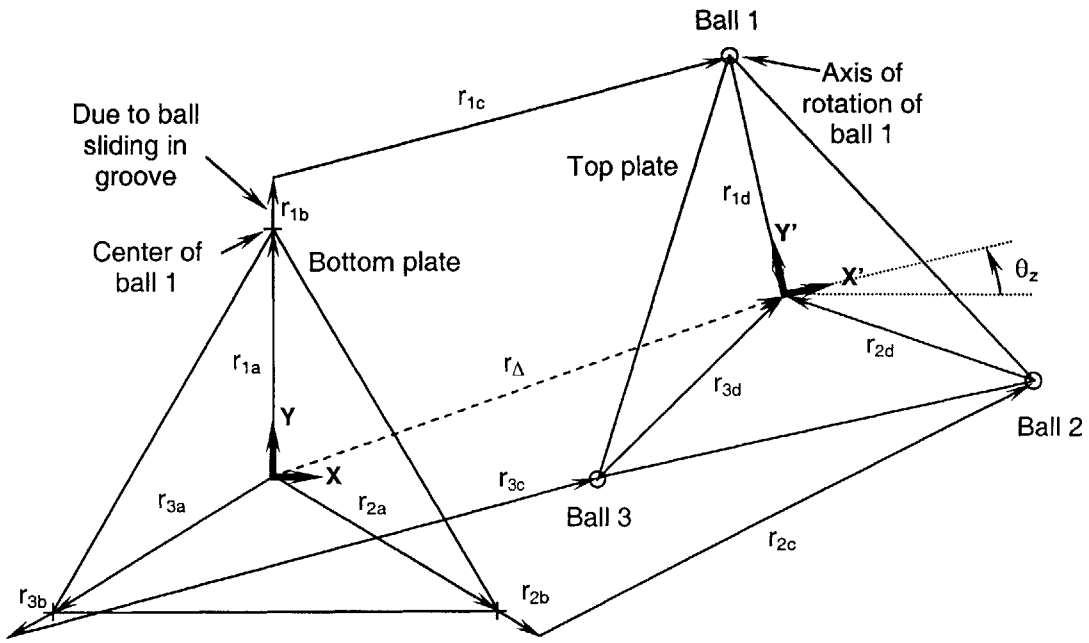

Figure 2.11 *– Vector loop model for in-plane motion of the ARKC*

It is important to be able to determine the new location and orientation of the centroid of the top plate after the balls rotate. This information is contained in vector $\vec{r}_\Delta$. Figure 2.11 shows three vector loops:

$$\begin{aligned} \vec{r}_{1a} + \vec{r}_{1b} + \vec{r}_{1c} + \vec{r}_{1d} &= \vec{r}_\Delta \\ \vec{r}_{2a} + \vec{r}_{2b} + \vec{r}_{2c} + \vec{r}_{2d} &= \vec{r}_\Delta \\ \vec{r}_{3a} + \vec{r}_{3b} + \vec{r}_{3c} + \vec{r}_{3d} &= \vec{r}_\Delta \end{aligned} \tag{2.1}$$

Each vector in Equation (2.1) is a two-dimensional vector $\vec{r} = r_x \cdot \hat{i} + r_y \cdot \hat{j}$, where $\hat{i}$ and $\hat{j}$ are unit vectors in the x and y directions respectively. Thus Equation (2.1) can be decomposed into a set of six nonlinear equations, which may be linearized assuming that the motion of the centroid of the coupling involves only small rotations about the three Cartesian axes (from linearization we approximate $\mathbf{sin}\,\theta \approx \theta$ and $\mathbf{cos}\,\theta \approx 1$). The linearized system of equations is shown in Equation (2.2) where **C**[θ] and **S**[θ] were used as shorthand notation for cosine and sine. Refer to the Appendix for a detailed derivation of Equation (2.2).

$$\begin{bmatrix} C[\theta_{1b}] & 0 & 0 & -1 & 0 & L_{1d}\,S[\theta_{1a}] \\ S[\theta_{1b}] & 0 & 0 & 0 & -1 & -L_{1d}\,C[\theta_{1a}] \\ 0 & C[\theta_{2b}] & 0 & -1 & 0 & L_{2d}\,S[\theta_{2a}] \\ 0 & S[\theta_{2b}] & 0 & 0 & -1 & -L_{2d}\,C[\theta_{2a}] \\ 0 & 0 & C[\theta_{3b}] & -1 & 0 & L_{3d}\,S[\theta_{3a}] \\ 0 & 0 & S[\theta_{3b}] & 0 & -1 & -L_{3d}\,C[\theta_{3a}] \end{bmatrix} \cdot \begin{pmatrix} L_{1b} \\ L_{2b} \\ L_{3b} \\ x \\ y \\ \theta_z \end{pmatrix} = \begin{pmatrix} (L_{1d}-L_{1a})C[\theta_{1a}]-L_{1c}\,C[\theta_{1c}] \\ (L_{1d}-L_{1a})S[\theta_{1a}]-L_{1c}\,S[\theta_{1c}] \\ (L_{2d}-L_{2a})C[\theta_{2a}]-L_{2c}\,C[\theta_{2c}] \\ (L_{2d}-L_{2a})S[\theta_{2a}]-L_{2c}S[\theta_{2c}] \\ (L_{3d}-L_{3a})C[\theta_{3a}]-L_{3c}\,C[\theta_{3c}] \\ (L_{3d}-L_{3a})S[\theta_{3a}]-L_{3c}\,S[\theta_{3c}] \end{pmatrix} \tag{2.2}$$

Equation (2.2) is of the form $A\cdot\vec{u}=\vec{b}$ where A and $\vec{b}$ are a 6×6 matrix and a 6×1 vector respectively and whose elements are known parameters. The vector $\vec{u}$ contains six unknowns; the first three correspond to sliding of the balls within the grooves as a result of the coupling changing configuration; the other three correspond to the new location and orientation of the top plate. The variables used in Equation (2.2) are defined in Table 2.2.

***Table 2.2** – Parameters for the in-plane model of the ARKC*

L_{ij} i=1,2,3 j=a,b,c,d	Length of vector $\vec{r}_{ij}$. The subscripts are as illustrated in Figure 2.11
θ_{ij} i=1,2,3 j=a,b,c,d	Orientation of vector $\vec{r}_{ij}$. All angles are measured with respect to the x axis and are positive in the counterclockwise direction
$\vec{r}_{ia}$	Vector from bottom plate centroid to center of ball i in the home configuration
$\vec{r}_{ib}$	Vector that defines amount ball i slides in groove i as a result of changing coupling configuration, i.e. rotating balls
$\vec{r}_{ic}$	Vector that defines the eccentricity of ball i. This vector points from the center of the ball to the axis of rotation of the ball
$\vec{r}_{id}$	Vector from the axis of rotation of ball i to the centroid of the top plate
$\vec{r}_{\Delta}$	Vector that defines in-plane motion of the coupling when the balls are rotated, i.e. when the coupling changes configuration

Figure 2.12 shows the relationship between a single ball input and displacement of the centroid of the top plate. The x displacement shown is achieved by varying θ_{1c} from 0° to 180° (note the near linear behavior around 90°). The nonlinear relationship between

θ_{1c} and displacement of the centroid indicates that an error in θ_{1c} has a different effect on the centroid displacement depending on the value of θ_{1c}. For example, an error of 1° in θ_{1c} when θ_{1c} is equal to 90° has a greater impact on the x location of the centroid of the coupling than the same error when θ_{1c} is equal to 0° or 180°. Most errors presented in the error budget of the ARKC in section 4.2 depend on the specific configuration of the coupling, that is, their magnitude varies as the balls are rotated. For the case of Figure 2.12, the eccentricity of the axis of rotation of each ball was taken at 127μm. The resulting resolution in the movement of the centroid of the coupling in the x direction near θ_{1c} equal to 90° is approximately 1.5 microns per degree.

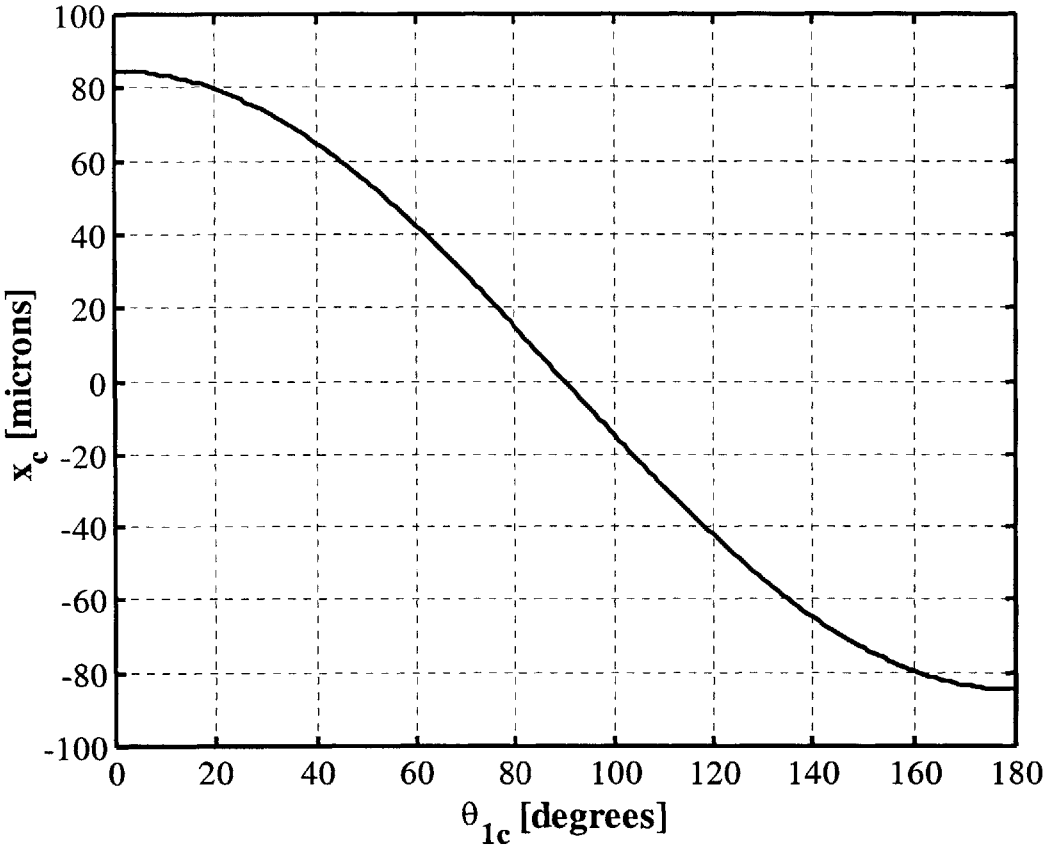

***Figure 2.12** – Motion of the centroid of the ARKC in the x direction*

Out-of-Plane Motion (z, θ_x, θ_y)

Out-of-plane displacements are as shown in Figure 2.13a; Figure 2.13b shows the coupling in its home configuration. Figure 2.13c shows a displaced configuration of the coupling achieved by translating the shafts attached to the balls. If all three shafts are extended or retracted in the same direction by the same amount, the end result is pure translation of the top plate in the z direction.

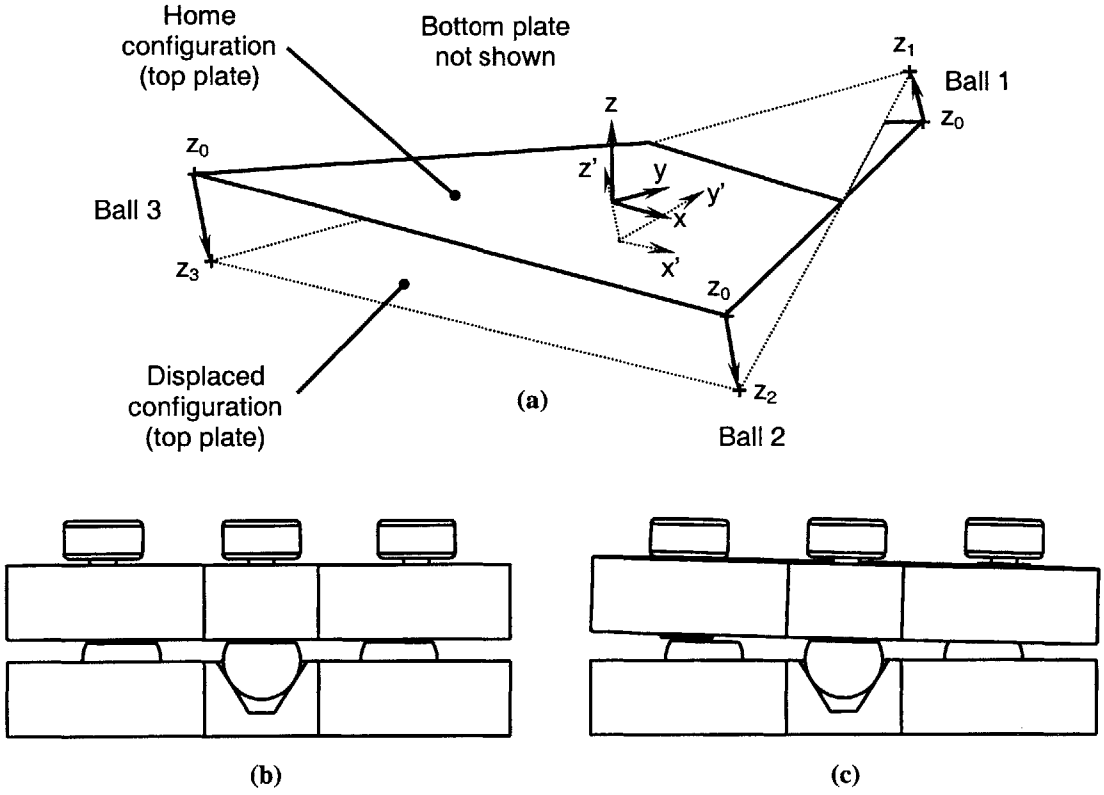

***Figure 2.13** – Out-of-plane motion of the ARKC: (a) model for out-of-plane motion; (b) home configuration; (c) displaced configuration*

It is of interest to find the new location and orientation of the centroid of the top plate after the shafts are translated. This information is obtained from the z coordinate of the center of each ball as seen in Figure 2.13a. The centers of the balls define a plane. Any normal vector to this plane contains information about the orientation of the plane with respect to a fixed coordinate system and thus the orientation of the centroid of the

coupling. For a symmetric three groove coupling, the z displacement of the centroid can be obtained by averaging the difference between a reference coordinate, say z_0, and the z coordinate of the center of each ball. The analysis is simplified by assuming that the motion of the shafts is limited in such a way as to allow only small displacements and rotations of the centroid of the coupling, i.e. small θ_x and θ_y. This assumption enables the use of the approximations $\mathbf{sin}\theta \approx \theta$ and $\mathbf{cos}\theta \approx 1$. The solution to this problem is documented by Culpepper in [3]. Equation (2.3) corresponds to the solution for a symmetric three groove coupling. A complete derivation can be found in the Appendix.

$$
\begin{aligned}
z_c &= \frac{(z_1 - z_0) + (z_2 - z_0) + (z_3 - z_0)}{3} \\
\theta_x &= -\frac{(z_2 - z_1)(x_3 - x_1) - (z_3 - z_1)(x_2 - x_1)}{(x_2 - x_1)(y_3 - y_1) - (x_3 - x_1)(y_2 - y_1)} \\
\theta_y &= \frac{(z_3 - z_1)(y_2 - y_1) - (z_2 - z_1)(y_3 - y_1)}{(x_2 - x_1)(y_3 - y_1) - (x_3 - x_1)(y_2 - y_1)}
\end{aligned}
\tag{2.3}
$$

The variables shown in Equation (2.3) are defined in Table 2.3.

***Table 2.3** – Parameters for the out-of-plane model of the ARKC*

x_i y_i z_i	Coordinates of the center of ball i
z_0	z coordinate of the center of all balls in the home configuration
z_c	z coordinate of the centroid of the top plate in the final configuration
θ_x θ_y	Orientation of the top plate in the displaced configuration

Applicability and Importance of Model

The model presented for in-plane and out-of-plane motion is an approximation to the exact mathematical model of the motion of the coupling. In this sense, the model is thus applicable only to small angle rotations of the centroid of the coupling (less than 5°) and its accuracy (better than 99%) is bound by the approximations $\mathbf{sin}\theta \approx \theta$ and $\mathbf{cos}\theta \approx 1$ for

θ_x, θ_y and θ_z. This model is valuable as a tool for quantifying the performance and the error budget of the coupling because the ARKC is intended to operate under such small rotations. In-plane and out-of-plane motions of the coupling can be treated independently as small displacements and rotations in-plane appear as second and higher order terms in out-of-plane analysis and vice versa.

Chapter 3

ARKC IMPLEMENTATION IN FLEXIBLE MANUFACTURING SYSTEMS

The adjustable and repeatable kinematic coupling discussed in the previous chapter has the ability to adjust its position in six degrees of freedom. This characteristic makes it suitable for automated fixturing and positioning applications in flexible manufacturing systems. The chapter starts with an overview of flexible manufacturing systems and industrial communication networks. These networks are important because they enable automation in manufacturing operations. The chapter continues with a discussion on the ways in which the ARKC addresses the fundamental issues described in the first chapter and ends with a discussion on the implementation of the ARKC in a flexible manufacturing system.

3.1 Flexible Manufacturing Systems and Industrial Communications Networks

Manufacturing enterprises have seen much progress in the area of flexible manufacturing systems (FMS) fueled by an ever-increasing demand for less expensive, more varied and higher quality products. A flexible manufacturing system is a highly automated system comprised of work cells capable of handling different manufacturing jobs in any specific order. Much of the progress has occurred in the last fifty years due in part to the advances in computer technology. In 1952, the world witnessed the invention of the first numerical

control machine. The first industrial robots appeared in the 1960's followed by integrated manufacturing systems in the 1970's. The 1980's brought about artificial intelligence, smart sensors and untended manufacturing cells. The decade of the 90's produced telecommunications and global manufacturing networks, fuzzy logic devices, artificial neural networks and internet tools [7].

Flexible manufacturing systems represent the highest level of productivity and efficiency in manufacturing plants because they combine the benefits of two other manufacturing systems: the high productivity of dedicated transfer lines and the high flexibility of job shops. Automation enables flexible manufacturing systems to [7]:

1. Integrate various aspects of manufacturing operations such as material handling, machining, testing, and assembly to improve product quality and uniformity, minimize cycle time and effort, and reduce labor costs.

2. Improve productivity by reducing manufacturing costs through better control of production. Parts are loaded, fed, and unloaded on machines more efficiently.

3. Improve quality by enabling more repeatable processes.

4. Reduce workpiece damage caused by manual handling of parts.

In the past, these benefits were not realized due to interoperability problems that existed between components of flexible manufacturing systems. Typically, manufacturing plants purchased components from several vendors and assembled them into automated cells. Communication between the components became a problem as each vendor employed proprietary control software with their equipment. The result was a mix of programmable devices which relied on a variety of processors and custom interfaces. This adversely increased complexity in manufacturing plants and often called for increased training of personnel. The problem compounded itself when the production line had to be reconfigured quickly by adding and replacing components.

These problems began to be addressed in 1980 with the development of the first set of communication standards collectively known as Manufacturing Automation Protocol (MAP). The International Organization for Standardization (ISO) created a reference model for Open System Interconnectivity (OSI). This model is accepted worldwide as the basis for all network communications and is known as ISO/OSI. It is based on a hierarchical structure in which communication between two users is divided into seven layers [8] as shown in Figure 3.1a. These layers can be grouped into application layers and transport layers according to their functionality. Application layers provide high-level functionality: layer 7 provides a uniform layer that abstracts the behavior of the network; layer 6 converts data formats between application representations and network representations; and layer 5 establishes sessions between machines. Transport layers deal with low-level operations: layer 4 splits data into messages to be transported; layer 3 routes the message packets; layer 2 breaks up and reassembles messages, and detects and corrects errors at the bit level; and layer 1 encodes and physically transfers the messages.

Several industrial communication networks such as the one shown in Figure 3.1b evolved from the ISO/OSI model. These networks seek to promote an open communication link between the different components that make up an automated manufacturing plant and resolve incompatibility problems between equipment from different vendors. Examples of these industrial communication networks are DeviceNet and Foundation Fieldbus. These examples are described below. A thorough discussion of these industrial communication networks can be found in references [9] and [10].

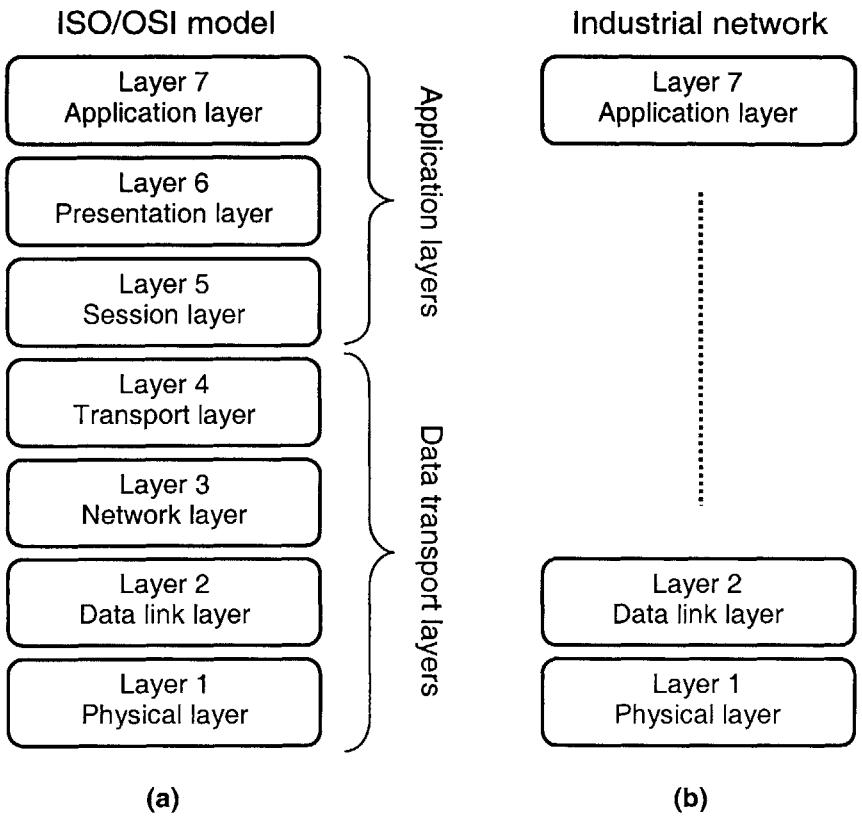

***Figure 3.1** – (a) ISO/OSI model for network communications; (b) most industrial communication networks do not use layers 3 through 6*

1. **DeviceNet** is a low-level network designed to connect industrial devices (sensors and actuators) to higher level devices (controllers). DeviceNet focuses on the interchangeability of low-cost, simple devices often used in manufacturing operations –such as limit switches, photoelectric sensors, motor starters, bar code readers, variable frequency drives, and operator interfaces.

   DeviceNet adds to the functionality of the ARKC by providing a way to operate the coupling in a flexible manufacturing system. Outfitting the ARKC with sensors and actuators compatible with DeviceNet guarantees its proper integration into a manufacturing system that relies on DeviceNet.

2. **Foundation Fieldbus** is a bi-directional communications protocol used for communications among field instrumentation and control systems. It is a serial all-digital link that serves as a local area network for factory instrumentation and control devices. It allows the introduction of new devices into the network without disrupting the network's active control functions. The main difference between Foundation Fieldbus and other device networks is the addition of a User Layer on top of the Application Layer of the ISO/OSI model. This extra layer performs control procedures at the field device as well as in the central controller [10].

   Foundation Fieldbus can be used to integrate and decentralize the overall control of an automated factory. In this way, the ARKC may be controlled by its specific controller as well as by controllers operating other machines. This in turn provides a redundant mechanism to sense and identify failure of the coupling and to adjust for wear. This added communication flexibility ensures the optimal adaptability and interchangeability of the ARKC in the manufacturing processes in which it is being used.

3.2 Addressing the Fundamental Issues

The fundamental issues described in section 1.3 are important in automated manufacturing operations requiring high accuracy and precision. Dealing with these issues appropriately results in greater productivity and lower production costs. The following paragraphs present each issue and explain how the ARKC addresses them.

Fundamental Issue #1: Provide automated micron-level repeatability and accuracy in precision couplings.

The ARKC provides micron-level repeatability because it is a kinematic coupling. Its accuracy depends on the sensors and actuators used to manufacture it and the control scheme used to operate it. Therefore, proper selection of these components ensures micron-level accuracy. Automation is achieved as a consequence of the coupling's adjustability (i.e. the actuators can be operated automatically).

Fundamental Issue #2: Improve manufacturing yield by in-process optimization of fixturing performance.

Manufacturing yield and manufacturing efficiency are two closely related concepts. Manufacturing yield refers to productivity (e.g. how many parts are produced per minute), whereas manufacturing efficiency refers to the time it takes to make something (e.g. how long does it take to make a part). In general, higher efficiency results in increased yield. A flexible manufacturing system is characterized by the efficiency of all the components in the system. Implementation of the ARKC in a flexible manufacturing system increases overall efficiency thus improving manufacturing yield in several ways. The ARKC:

1. Provides a fast and repeatable mechanism to load and unload parts.

2. Extends the functionality of a conventional fixture by allowing it to be used in different operations such as machining, testing and assembly. A workpiece stays attached to its fixture until completion and all operations are performed without multiple setup steps on different fixtures specifically designed for each operation.

3. Can help increase the routing flexibility of a manufacturing plant. Each coupling on the manufacturing floor can be marked with a tag. The tag may be a magnetic strip, a bar code sticker or a RF transmitter attached to the piece. The tag contains information about the part affixed to the coupling and can therefore be used to determine how to handle and operate on such part. In this way, some operations can be performed off the main conveyor line on specific parts and when completed they can be fed back into the main line [11].

4. Decreases the statistical variation of manufactured parts by improving repeatability and enabling active error compensation.

Fundamental Issue #3: Provide active error correction to compensate for time variable errors in detachable fixtures.

A static detachable fixture cannot actively compensate for time variable errors. This fixture can be made active by incorporating an ARKC. The adjustability of the ARKC in six degrees of freedom gives the fixture the ability to accurately position a workpiece and to actively compensate for time variable errors due to wear and temperature variations provided these errors can be measured.

Fundamental Issue #4: Provide precision fixturing with multiple states of assembly.

Multiple states of assembly mean variations in the location of features in a part. For example, consider a family of parts with a hole located at varying distances from one of the faces of the part. Conventional flexible fixturing may be used to produce such parts in batches. The fixture is setup for part A, the part is produced and a new identical part is setup in the fixture to repeat the process over again. When part B, which is similar to part A but has the hole at a different distance from the face, needs to be produced, the fixture has to be reconfigured. The ARKC can provide this functionality automatically without having to configure the fixture every time.

3.3 ARKC Implementation

This section presents a manufacturing scenario to illustrate the use of the ARKC and to show how the ARKC addresses the fundamental issues described in section 1.3. The scenario assumes that the manufacturing system under consideration is a flexible manufacturing system and that part features have to be located with tolerances on the order of 5μm. Figure 3.2 shows the process flow for the use of the ARKC as envisioned in a typical manufacturing scenario.

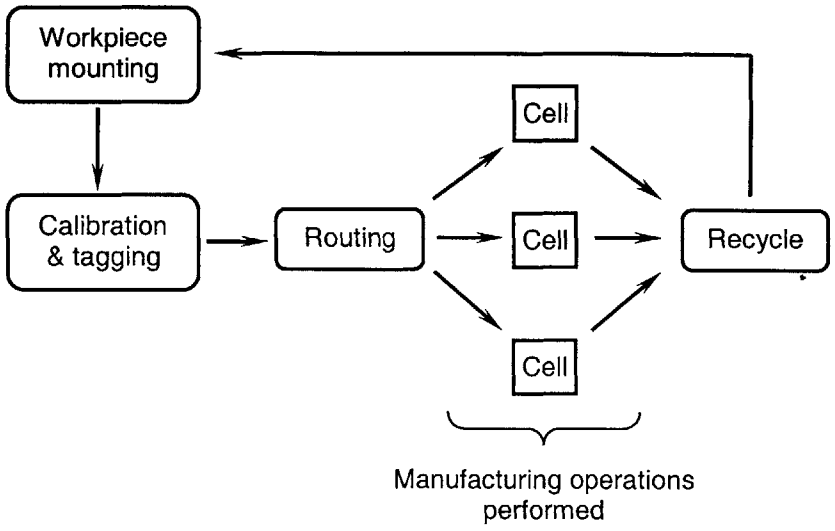

Figure 3.2 – Process flow to illustrate the use of the ARKC in a manufacturing scenario

3.3.1 Workpiece Mounting

The workpiece is mounted on the groove plate of the ARKC to avoid the need to move actuators with the workpiece. Plates with the actuated balls can be integrated into the different machines on the manufacturing floor. Ideally, the grooves are machined into the workpiece although an intermediate interface may be used as shown in Figure 3.3. If used, this interface must meet two functional requirements:

1. It must maintain the relative orientation between the workpiece and the groove plate.

2. It has to prevent excessive deformations due to machining forces.

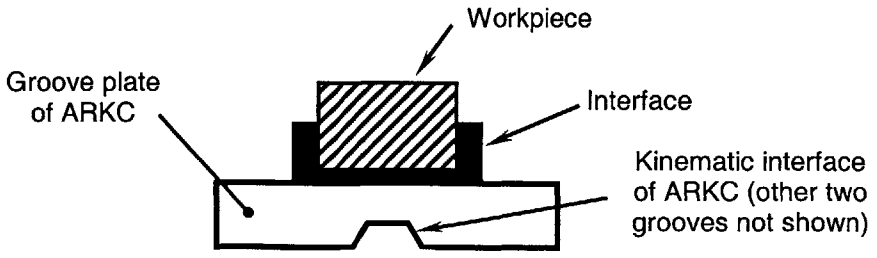

Figure 3.3 – Workpiece mounting on ARKC

3.3.2 Calibration and Tagging

The goal of this step is to determine the coordinate transformation from a reference coordinate system in A to a reference coordinate system in B as shown in Figure 3.4. This transformation is determined by measuring the relative position and orientation of reference coordinate systems A and B. If a calibration plate is rigidly attached to ground (e.g. a granite table), the position and orientation of the reference coordinate system of body B may be determined by using a coordinate measuring machine (CMM).

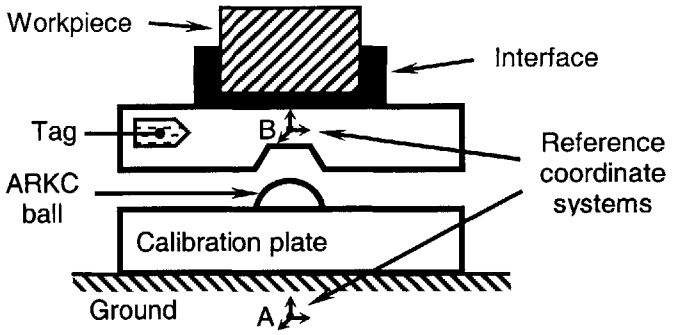

Figure 3.4 – Calibration and tagging of the ARKC

Information about the workpiece and the coordinate transformation from A to B is referenced to the tag attached to B. The control system saves this information, associates it with the tag and uses it to identify the workpiece. After calibration and tagging, the workpiece, fixture and groove plate are released into the production line as one rigid body.

3.3.3 Routing

The workpiece is routed to specific manufacturing cells as it travels along the production line. Routing decisions are driven by the manufacturing operations that need to be performed and the state of the cells in the plant. These decisions can be made at the overall control system level or at the conveyor level depending on the type of decision. For example, the control system can make a decision about redirecting the workpiece into a less busy cell and the conveyor can make a decision about redirecting the workpiece to

a specific machine depending on the operation to be performed on it. Both DeviceNet and Foundation Fieldbus enable such control scheme.

3.3.4 Manufacturing Operations

The process of loading a workpiece on a machine proceeds as follows:

1. The machine identifies the workpiece via the tag attached to the groove plate of the ARKC.

2. The machine arranges the ARKC balls to position the workpiece using the calibration information. In order to prevent excessive wear of the kinematic interfaces, the balls should be arranged before the coupling is engaged. The micron-level repeatability of the kinematic coupling guarantees the accurate position of the workpiece after engagement.

3. The ARKC is brought together and a preload force is applied to hold the two plates in place.

3.3.5 Recycle of Couplings and Coupling Failure

Once all manufacturing and assembly operations are finished, the workpiece is removed from the groove plate which is then recycled. The determination on whether to reuse the fixture depends on several factors. The grooves and balls go through a wear-in period in which the repeatability of the coupling changes. After this wear-in period, the repeatability of the coupling improves by a factor of two to three [12]. The grooves and balls may fail after a certain number of cycles depending on whether lubrication is used and whether the machine is crashed. Crashing the machine may permanently deform the kinematic interfaces of the coupling decreasing its repeatability. The coupling interface attached to or built into the machines (i.e. balls) can be made of a much harder material than the grooves and thus last significantly longer.

Chapter 4

ARKC PERFORMANCE, ERROR BUDGET AND OTHER DESIGN CONSIDERATIONS

4.1 Performance

The ARKC was conceived for applications requiring repeatability around 1μm and accuracy of about 5μm. Designing the coupling with six points of contact (exact constraint design) gives the coupling excellent repeatability in six degrees of freedom. Equipping the coupling with actuated mechanisms, gives the coupling adjustability and thus enables accuracy. Proper design of the contact interfaces and careful material selection ensures a desired coupling stiffness. These measures of performance – repeatability, accuracy and stiffness– are fundamental to every kinematic coupling and fixture. This section presents modeling techniques for estimating the repeatability, the accuracy and the stiffness of the ARKC based on established kinematic coupling theory and the adjustable kinematics theory developed earlier in this thesis. These techniques are applied in the case study presented in the next chapter.

4.1.1 Optimizing the Repeatability of a Kinematic Coupling

Methods for determining the contact stiffness of kinematic couplings are well established. Our primary concern is in addressing the optimization of the couplings' performance.

The following is a brief description of recent work that provides the theory and methods for optimizing coupling function [13]. When a kinematic coupling is initially engaged, points in the balls make contact with their corresponding grooves. Each new contact point forces the coupling into an increasingly resistive engagement path until five such contact points (out of possible six) are established. At this point the coupling is left with one degree of freedom as shown in Figure 4.1. This degree of freedom allows the coupling to move in a particular direction provided the other five points of engagement are free to slide. Thus, a nesting or preload force acting to bring the coupling together initially causes five engaged contact points to slide. When the sixth contact engages the coupling becomes fully constrained.

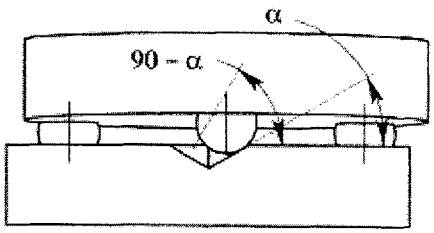

***Figure 4.1** – Kinematic coupling with five constraints engaged [13]*

An indicator for the trend of planar repeatability [13] of a standard three groove coupling is given in Equation (4.1). The expression quantifies the repeatability (ρ) of the coupling based on the groove angle (α), coefficient of friction (μ), normal stiffness at the contact points (k_{zz}) and preload force (F) normal to the plane of the coupling.

$$\rho \approx \frac{\mu F}{18 k_{zz} \sin^2 \alpha \cos \alpha} \left(2\sqrt{3} + \cos \alpha + \sin 2\alpha\right) \tag{4.1}$$

It follows from Equation (4.1) that the repeatability of the coupling can be improved by decreasing the coefficient of friction and by increasing the stiffness of the contact points. Decreasing the preload also improves repeatability but has an adverse effect on stiffness. If parameters μ, F and k_{zz} are fixed, the coupling achieves its best repeatability when α is equal to 58°.

4.1.2 Optimizing Coupling Accuracy

The accuracy of the ARKC depends on the positioning resolution of the actuators. It can be quantified by discretizing the corresponding quantities in the mathematical model of the coupling motion as given in Equations (2.2) and (2.3). For in-plane motion, an angular resolution of $\Delta\theta_{ic}$ discretizes the values that θ_{ic} can take in Equation (2.2) and thus discretizes the in-plane working volume of the coupling. Similarly, a linear resolution of Δz_i discretizes the values that z_i can take in Equation (2.3) and thus discretizes the out-of-plane working volume of the coupling. The largest difference between a desired coupling configuration and an adjacent point in such discretized working volume corresponds to the worst case accuracy of the coupling. It follows from the previous discussion that as the resolution of the actuators improves so does the accuracy of the coupling. This of course is limited by friction hysteresis and interactions between surface irregularities at the contact points (i.e. surface finish).

4.1.3 Optimizing Coupling Stiffness

All bodies deform under the influence of forces. According to Hertz theory as reported in [14], point contacts in non-conforming solids become ellipses when loaded. The load-displacement characteristics of the contact region, and thus the stiffness, can be calculated from the theory as given by Equation (4.2). In Equation (4.2), δ is the mutual approach of two distant points in the contacting solids, F is the preload force compressing the solids, and R_e and E_e stand for the equivalent radius and equivalent modulus of elasticity of the contact region. Expressions for R_e and E_e are presented in the next chapter in Equations (5.2) and (5.3) on page 73.

$$\delta = \left(\frac{9F^2}{16R_e E_e^2} \right)^{1/3} \tag{4.2}$$

The stiffness at each contact point can be expressed in matrix form. Assuming that the local coordinate system at each contact is oriented with the z axis normal to the plane of contact (plane tangent to ball and groove at contact point), the resultant stiffness matrix

has only one non-zero element as shown in Equation (4.3). This non-zero element corresponds to the contact stiffness k_{zz} calculated from Hertz theory. The subscript ℓ stands for "local" meaning that $(K_\ell)_i$ is the stiffness matrix, as seen from the local coordinate system, at contact point i.

$$K_\ell = \begin{bmatrix} 0 & 0 & 0 & 0 & 0 & 0 \\ 0 & 0 & 0 & 0 & 0 & 0 \\ 0 & 0 & k_{zz} & 0 & 0 & 0 \\ 0 & 0 & 0 & 0 & 0 & 0 \\ 0 & 0 & 0 & 0 & 0 & 0 \\ 0 & 0 & 0 & 0 & 0 & 0 \end{bmatrix} \tag{4.3}$$

Among other factors, the contact stiffness depends on the shape of the two bodies making contact (e.g. cylinder in contact with plane, ball in contact with cylinder, etc.) and on the materials of these two bodies. Therefore, k_{zz} can be optimized by choosing appropriate materials and by changing ball-grove geometry.

The kinematic coupling, having six points of contact, has six local stiffness matrices. Each of these can be expressed in a global coordinate system CS_g (e.g. the coordinate system used for the centroid of the coupling) by transforming it with the appropriate transformation matrix $T_{g/\ell}$. The global stiffness matrix for the kinematic coupling is obtained by adding the six transformed stiffness matrices as shown in Equation (4.4). This procedure is illustrated in detail in the references [13] and [15].

$$K_g = \sum_i \left((T_{g/\ell})_i \cdot (K_\ell)_i \cdot (T_{g/\ell})_i^T \right) \tag{4.4}$$

The global stiffness matrix contains information about the stiffness of the kinematic coupling in six axes: x, y, z, θ_x, θ_y and θ_z. The stiffness of other components is equally important in the ARKC. In addition to the analysis just described, it is necessary to quantify the stiffness of the bearings used to support the shafts. This is important as the stiffness of these bearings can be orders of magnitude lower than the contact stiffness due to Hertz contact and thus account for an overall decreased coupling stiffness. If the

bearing-shaft stiffness is over ten times that of the ball-groove joint stiffness, then the ball-groove joint stiffness will dominate the coupling's overall stiffness. It is therefore assumed that proper design practice has been followed and that errors due to the bearing-shaft interface are negligible compared to the ball-groove errors.

4.2 Error Budget

It is impossible to design and manufacture a system with zero tolerance, zero backlash and perfect surface finish. It is also impossible to maintain perfect control over errors induced by thermal and vibration perturbations. The error budget is a valuable analysis tool that allows the design engineer to meet the performance requirements of a system by allocating specific amounts of error to the components and interfaces that make up the system.

This section presents the error budget of a 120° three-groove ARKC such as the one shown in Figure 2.9. Only the major error contributions have been modeled in the interest of simplicity.

4.2.1 Errors Due to Manufacturing Tolerances

The principal source of error related to manufacturing tolerances occurs in the location of the axis of eccentricity of each ball with respect to the center of the ball as seen in Figure 4.2. This source of error affects only in-plane motion of the coupling and can be quantified (via worst case estimation) by adding or subtracting the magnitude of the error to L_{ic} in Equation (2.2).

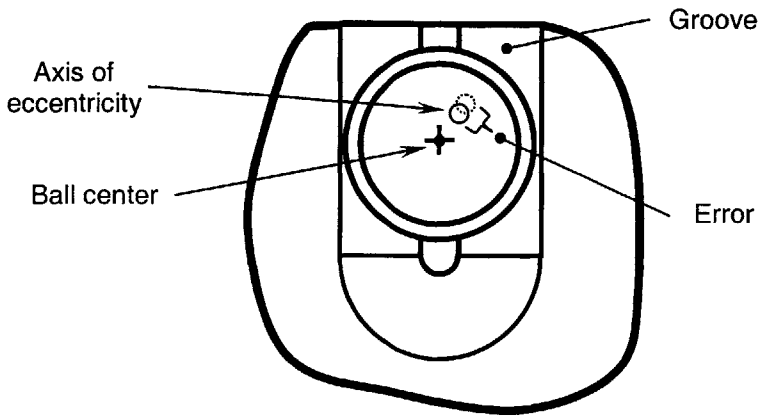

***Figure 4.2** – Error in radial location of the axis of eccentricity of a ball with respect to the center of the ball*

Note that the impact this error has on the accuracy of the coupling varies with the angular position of each ball. That is, some coupling configurations are more sensitive to this error than others. Table 4.1 quantifies this error via an example and shows the most sensitive configurations.

***Table 4.1** – Worst case errors due to manufacturing tolerances*

Characteristics	Eccentricity $L_{ic} = 127\,\mu m$ [0.005 in] Eccentricity error $\Delta L_{ic} = \pm 12.7\,\mu m$ [$\pm$0.0005 in]
Maximum sensitivity	Error δx is maximum when: $\theta_{1c} = 0°$, $\theta_{2c} = 60°$ and $\theta_{3c} = 300°$ or $\theta_{1c} = 180°$, $\theta_{2c} = 240°$ and $\theta_{3c} = 120°$ Error δy is maximum when: $\theta_{1c} = 90°$, $\theta_{2c} = 60°$ and $\theta_{3c} = 120°$ or $\theta_{1c} = 270°$, $\theta_{2c} = 240°$ and $\theta_{3c} = 300°$ Error $\delta\theta_z$ is maximum when: $\theta_{1c} = 0°$, $\theta_{2c} = 240°$ and $\theta_{3c} = 120°$ or $\theta_{1c} = 180°$, $\theta_{2c} = 60°$ and $\theta_{3c} = 300°$

Results	Maximum error at centroid: $\delta x_{max} = \pm 16.9 \mu m \; [\pm 6.7 \times 10^{-4} \text{ in}]$ $\delta y_{max} = \pm 14.7 \mu m \; [\pm 5.8 \times 10^{-4} \text{ in}]$ $(\delta \theta_z)_{max} = \pm 166 \mu rad \; [\pm 9.5 \times 10^{-3} \text{ deg}]$

Although these errors appear large for a precision coupling, they can be mapped and effectively removed from the coupling behavior using control. Manufacturing and assembly errors are systematic measurable errors.

4.2.2 Errors Due to Bearing Runout

The bearings shown in Figure 4.3 must allow axial and rotational movement of the shaft in order for the ball to have the required two degrees of freedom. Errors in the radial or axial location of the shaft result in "accuracy errors" in the coupling. Axial errors can be corrected by the actuators whereas radial errors due to bearing runout cannot be practically addressed. The bearings that support the shafts of the coupling are therefore a critical component and special care must be taken in their selection in order to meet the performance requirements for the coupling.

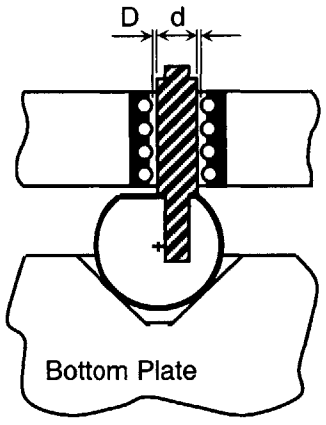

Runout = f(D – d, surface finish,
ball-shaft size,
lubrication, speed,
etc.)

Figure 4.3 – Bearing runout

Bearing runout affects in-plane accuracy of the coupling. These errors may be independent of the coupling configuration (i.e. they may not depend on the angular position of each ball). The error can be incorporated into the kinematic model by adding (or subtracting) it to L_{ic} in Equation (2.2). Following the logic in Table 4.1, the maximum error displacements of the coupling in x and y can be quantified by setting θ_{ic} to 0° or 90° respectively. Note that errors in x and y displacements are independent of the diameter of the coupling while errors in θ_z are not. Table 4.2 quantifies these errors in via an example.

***Table 4.2** – Errors due to bearing runout*

Characteristics	Eccentricity $L_{ic} = 127\,\mu m$ [0.005 in] Runout error $\Delta L_{ic} = \pm 2.5\,\mu m$ [$\pm 1 \times 10^{-4}$ in] Coupling diameter $d = 152\,mm$ [6 in]
Results	Maximum error at centroid: $\delta x_{max} = \pm 2.5\,\mu m$ [$\pm 1 \times 10^{-4}$ in] $\delta y_{max} = \pm 2.5\,\mu m$ [$\pm 1 \times 10^{-4}$ in] $(\delta\theta_z)_{max} = \pm 40\,\mu rad$ [$\pm 2.3 \times 10^{-3}$ deg]

4.2.3 Errors Due to Contact Stresses

Contact forces cause deformations between far field points in the balls and grooves as shown in Figure 4.4. This deformation accounts for a finite displacement at the centroid of the coupling. Variations in the preload force cause variations in the position of the centroid. Slocum created a spreadsheet to calculate the errors in the position of the centroid of a three groove kinematic coupling given coupling characteristics and loading conditions [16]. The results of this spreadsheet analysis are shown on Table 4.3 for an example application of the contact errors in an ARKC.

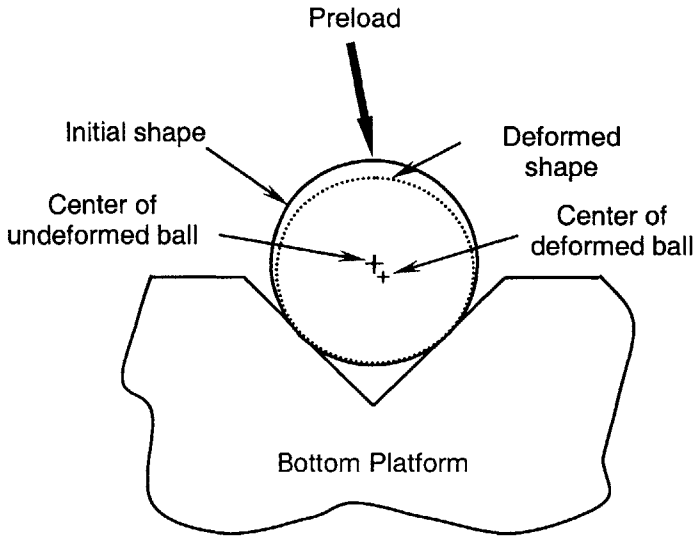

***Figure 4.4** – Error due to contact stresses at balls*

***Table 4.3** – Errors due to contact stresses at balls*

Characteristics	Major radius of the ball $R_{major} = 12.7\,\text{mm}$ [0.5in]
	Minor radius of the ball $R_{minor} = 12.7\,\text{mm}$ [0.5in]
	Groove radius $R_{groove} = \infty$
	Groove angle $\alpha = 45°$
	Material properties for balls and grooves:
	RC-62 steel
	Modulus of elasticity $E = 204\,\text{GPa}$ [29.5×10^5 psi]
	Poisson ratio $\nu = 0.29$
	Coupling diameter $d = 15.2\,\text{mm}$ [6in]
	Preload force $F = 450\,\text{N}$ [101lbf]
	Variation in preload $\Delta F = \pm 22.5\,\text{N}$ [± 5.0lbf]
Results	Error in centroid location $\delta z = \pm 0.1\mu\text{m}$ [$\pm 4\times10^{-6}$ in]

Errors due to contact stresses at balls and grooves are systematic given that the error in preload can be measured.

4.2.4 Errors Due to Actuator Errors

There are two types of errors introduced by the actuators: in-plane errors and out-of-plane errors. In-plane errors are caused by errors in the angular positioning capabilities of the actuators. If stepper motors are used to rotate each ball, the angular orientation of the balls is known within the precision limits of the stepper motors. If servo motors are used instead, the angular orientation of the balls is known within the precision limits of the motors and the servo control feedback loop. In-plane errors due to actuator errors are dependent on the coupling geometry and on the angular position of each ball. These errors enter Equation (2.2) as errors in θ_{ic}. Table 4.4 shows numerical results for an example application using a common type of stepper motor.

***Table 4.4** – In-plane errors due to actuator errors*

Characteristics	Step size: 0.225° Step error ($\pm 50\%$ of step size): $\pm 0.1125°$ Coupling diameter $d = 15.2\,\text{mm}$ [6 in]
Maximum sensitivity	Error δx is maximum when: $\theta_{1c} = 90°$, $\theta_{2c} = 150°$ and $\theta_{3c} = 30°$ or $\theta_{1c} = 270°$, $\theta_{2c} = 330°$ and $\theta_{3c} = 210°$ Error δy is maximum when: $\theta_{1c} = 0°$, $\theta_{2c} = 330°$ and $\theta_{3c} = 30°$ or $\theta_{1c} = 180°$, $\theta_{2c} = 150°$ and $\theta_{3c} = 210°$ Error $\delta\theta_z$ is maximum when: $\theta_{1c} = 90°$, $\theta_{2c} = 330°$ and $\theta_{3c} = 210°$ or $\theta_{1c} = 270°$, $\theta_{2c} = 150°$ and $\theta_{3c} = 30°$

Results	Maximum error at centroid: $\delta x_{max} = \pm 0.33\,\mu m\ [\pm 1.3\times 10^{-5}\ in]$ $\delta y_{max} = \pm 0.28\,\mu m\ [\pm 1.1\times 10^{-5}\ in]$ $(\delta\theta_z)_{max} = \pm 3.2\,\mu rad\ [\pm 1.9\times 10^{-4}\ deg]$

Out-of-plane errors are caused by errors in the linear positioning capabilities of the actuators. They depend on the coupling geometry (e.g. coupling diameter) and on the z coordinate of the center of each ball. Table 4.5 shows numerical results for an example application.

***Table 4.5** – Out-of-plane errors due to actuator errors*

Characteristics	Step size: $10\,\mu m\ [3.9\times 10^{-4}\ in]$ Step error ($\pm 50\%$ of step size): $\pm 5\,\mu m\ [\pm 1.9\times 10^{-4}\ in]$ Coupling diameter: $d = 15.2\,mm\ [6 in]$
Maximum sensitivity	Maximum sensitivity when the ball centers have the same z coordinate (i.e. when they lie on a horizontal plane)
Results	Maximum error at centroid: $\delta z_{max} = \pm 5\,\mu m\ [\pm 1.9\times 10^{-4}\ in]$ $(\delta\theta_x)_{max} = \pm 87\,\mu rad\ [\pm 5.0\times 10^{-3}\ deg]$ $(\delta\theta_y)_{max} = \pm 75\,\mu rad\ [\pm 4.3\times 10^{-3}\ deg]$

4.3 Other Design Considerations

The stiffness of the ARKC depends on the stiffness of its components. It is important to balance the stiffness of individual components (so as to not overstress them) while maximizing the overall coupling stiffness. Conventional kinematic couplings can be made nearly monolithic because they do not have moving components. The ARKC, on the other hand, has to be designed carefully because it contains moving parts and the contact stiffness and friction between these moving parts can be sources of compliance

errors and random contact errors. In the same way, it is important to pay careful attention to the transmission of forces and torques from the actuators to the moving components of the coupling to minimize parasitic error motions. For example, if a dual-motion actuator is used to rotate and push one of the balls of the coupling, the connection between the actuator and the ball (e.g. via shafts) must be designed carefully to avoid transmitting actuator runout error motions to the ball. The connection must allow transmission of motion in two directions and must isolate the ball from errors in the other four directions. This connection can be achieved with a properly designed flexure such as the one shown in Figure 4.5.

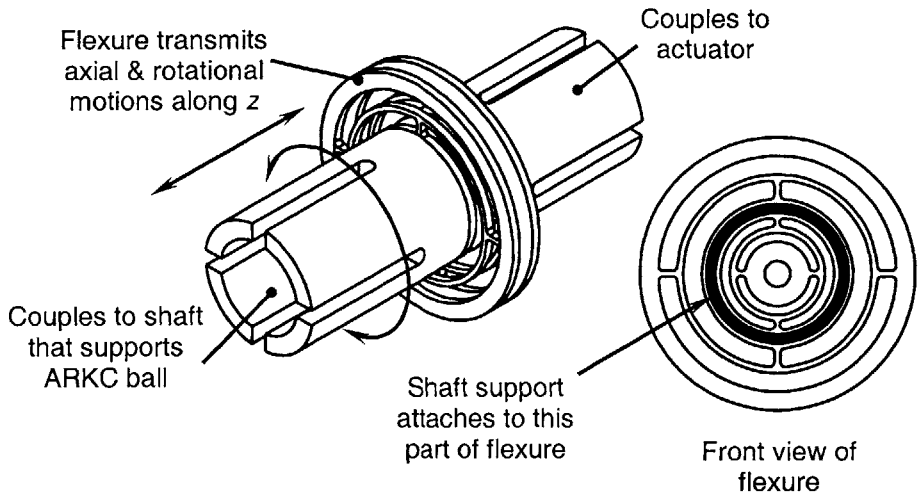

***Figure 4.5** – Flexure to isolate actuator error motions [ball (not shown) between spliced shafts support load along coupling axis]*

Different levels of performance may be achieved by using different components. Accuracy on the order of 5μm and repeatability on the order of 1μm can be attained by using air bushings to support the shafts. This configuration is best used when loads on the coupling are very low. In essence, this design trades a lower stiffness for improved performance via reduction in random errors (i.e. runout). Accuracy on the order of 25μm and repeatability on the order of 5μm can be attained by replacing the air bushings with ball bushings. A ball bushing gives the coupling higher stiffness compared to air bushings but increases the friction in the system. Thus this design is better suited for high-load applications. Better performance requires the use of a flexure to minimize

random/parasitic errors. For instance, consider the flexure based design shown in Figure 4.5. Combining such a flexure with piezoelectric actuators may result in accuracy on the order of 1μm and sub-micron repeatability. Table 4.6 summarizes the expected accuracy and repeatability from a coupling made with different components.

***Table 4.6** – Effect of component selection on ARKC performance*

Components	**Linear*** **Accuracy [μm]**	**Linear Repeatability [μm]**
Piezo actuators Flexures	1 – 5	~ 1
Dual motion actuator Air bushings	5 – 25	1 – 5
Open loop stepper motor Ball bushing or contact bushing	> 25	> 5

4.4 Experimental Results

An adjustable and repeatable kinematic coupling was built and tested for in-plane motion and repeatability. Rodríguez's thesis, "Design and Manufacturing of an ARKC" [2], documents the most important experimental results. The coupling tested by Rodríguez was optimized for better performance and tested again for the results of this thesis. The two most important modifications made during the optimization were: the stiffness of the ball-shaft interface was increased and the flexure design shown in Figure 4.5 was used (replacing a hard coupling) to better isolate the balls from error motions in the actuators.

This coupling had a diameter of 15.2mm. For ball 1, the distance between the axis of rotation and the center of the ball (i.e. eccentricity) was 165μm; for ball 2, the eccentricity was 318μm; and for ball 3 the eccentricity was 368μm.

---

* Note: Angular accuracy and repeatability are not provided as they depend on other coupling characteristics (e.g. geometry)

Figure 4.6 compares theoretical and experimental motion of the centroid of the coupling in the x direction. The test consisted in homing balls 2 and 3 (i.e. ball 2 at 330° and ball 3 at 210°) and rotating ball 1 by ±18° from its home position (i.e. 90°). A larger range of testing was impossible due to the limited range of the capacitance probes used to measure displacement.

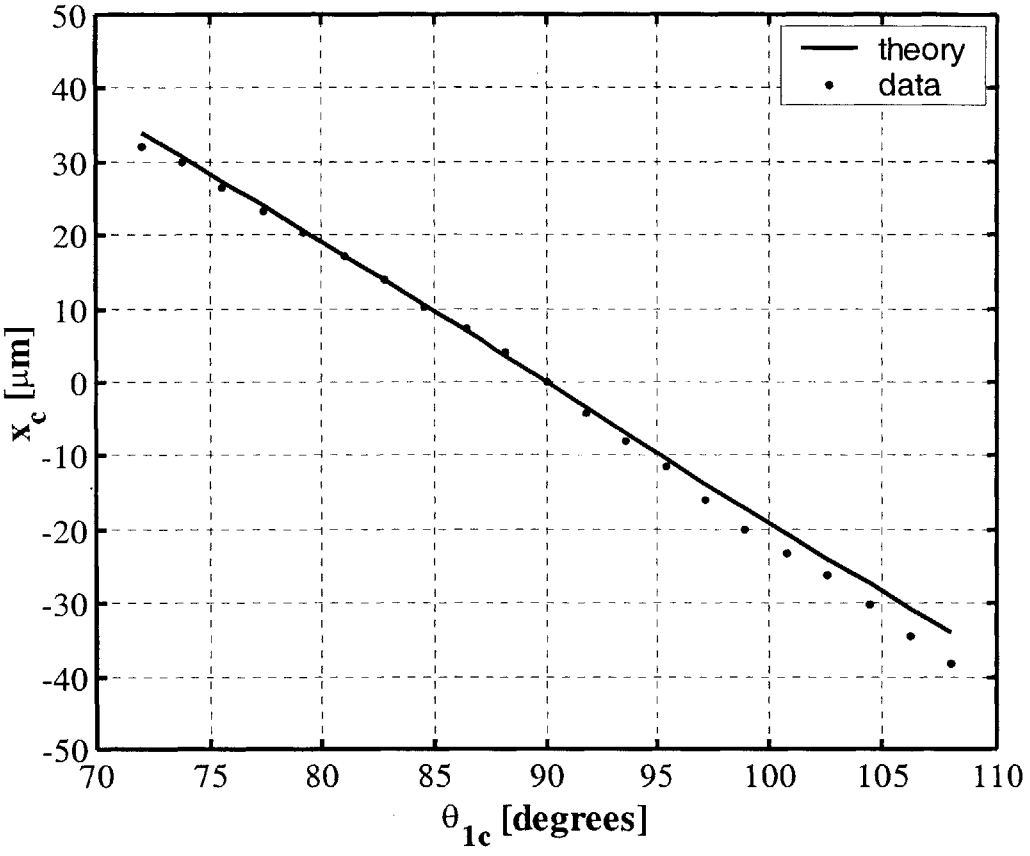

***Figure 4.6** – Motion of the centroid of the coupling in the x direction*

Figure 4.7 compares theoretical and experimental motion of the centroid of the coupling in the y direction. The test consisted in homing ball 1 (i.e. ball 1 at 90°) and rotating balls 2 and 3 by ±14.4° from their home position (i.e. 90°) in opposite directions. The abscissa in Figure 4.7 corresponds to rotation of ball 3.

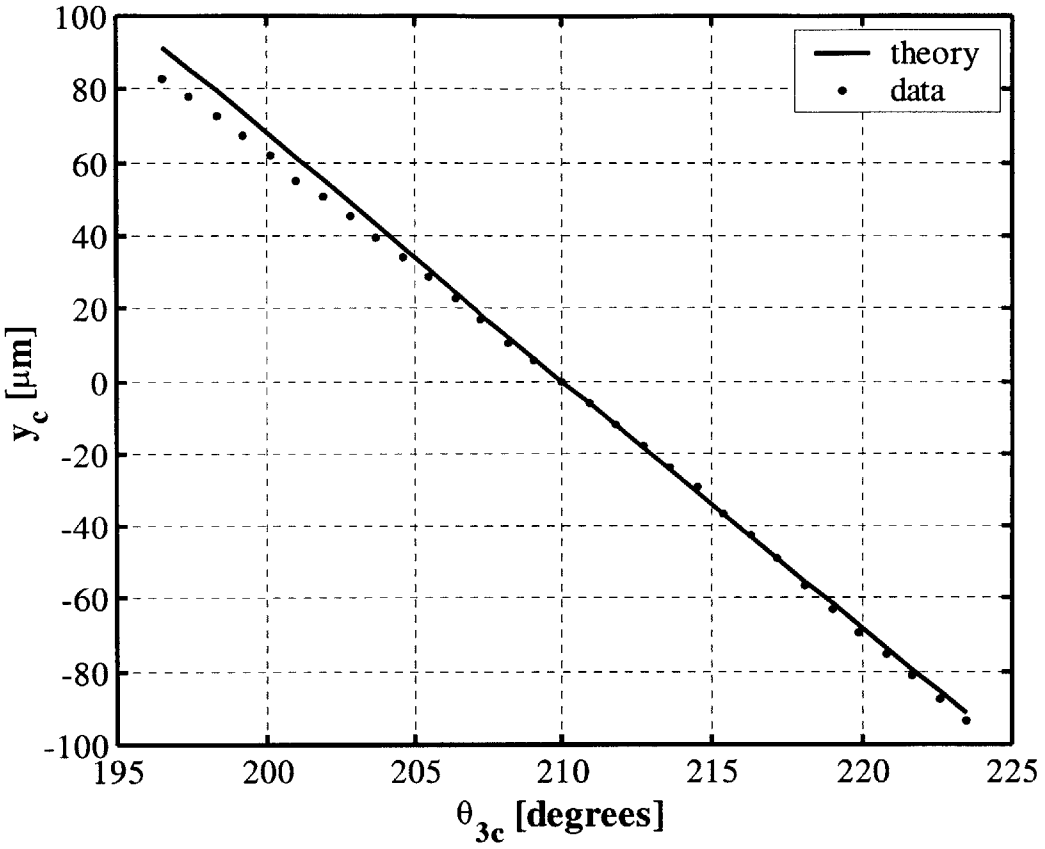

***Figure 4.7** – Motion of the centroid of the coupling in the y direction*

Figure 4.8 compares theoretical and experimental motion of the centroid of the coupling in θ_z. The test was the same as for Figure 4.6.

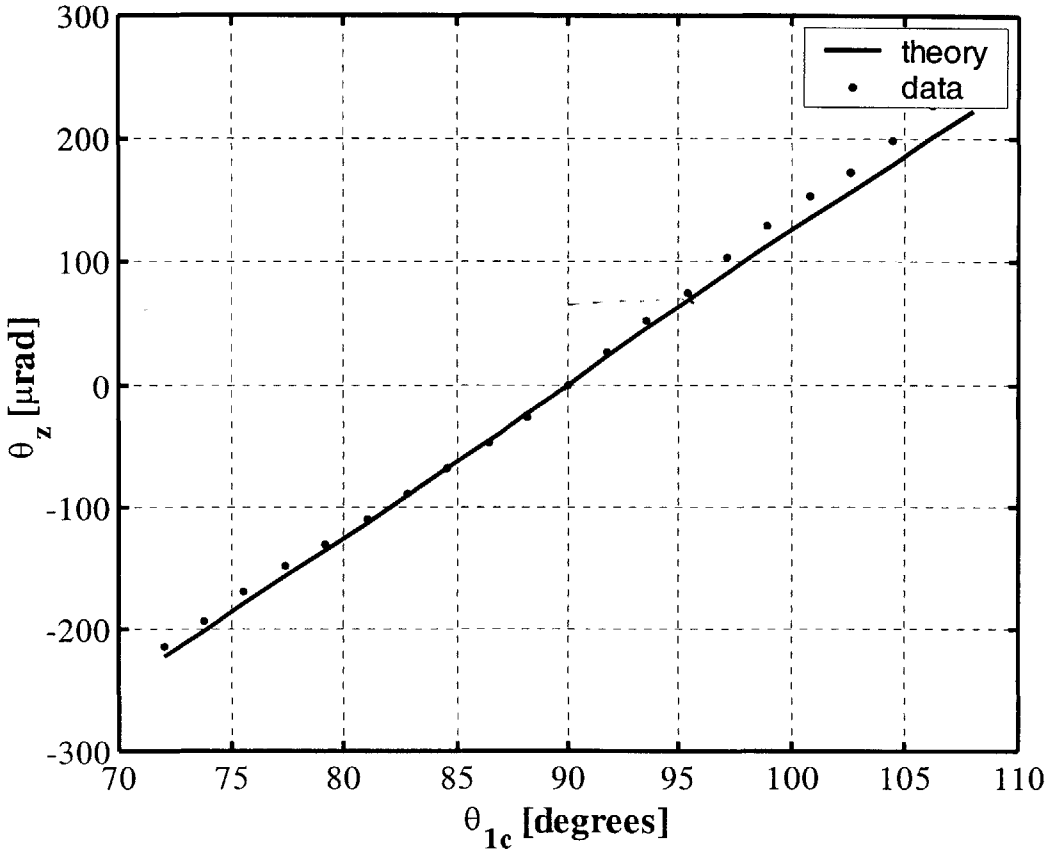

***Figure 4.8** – Motion of the centroid of the coupling in* θ_z

Data sets for out-of-plane displacements show similar results, but are not included due to space limitations. Random errors due to friction and surface irregularities were quantified at less than 2μm via repeatability tests. Bearing run-out contributes to random errors and was measured at 1.5μm. Due to the limitations of the capacitance probe's measurement range, we were not able to take data over the fully actuated range for each ball (+/- 90° from home position). A planned reduction of eccentricity will allow us to measure performance over the entire work volume. Systematic errors were less than 13% and likely due to error in the measurement of eccentricities and ball-groove size and placement. Fortunately, the systematic errors can be mapped and eliminated through compensation techniques.

Chapter 5

CASE STUDY: ADJUSTABLE KINEMATIC DOCKING SYSTEM

5.1 Introduction

This chapter covers a case study on an adjustable kinematic docking system for use in aligning semiconductor test equipment. The goal of this chapter is to illustrate how design concepts adopted from the ARKC can be applied to a precision fixturing application in order to increase functionality.

The chapter includes the following topics:

1. Brief overview of the process and equipment to test integrated circuits.
2. Discussion of three existing docking system designs: breech-lock, pull-down block and kinematic docking system (KDS).
3. Design of an adjustable kinematic docking system (AKDS) based on the kinematic docking system (KDS). This section illustrates how concepts adopted from the ARKC add to the functionality of the KDS.
4. Expected results. This section discusses the expected results based on the analysis presented in the previous chapter. The repeatability, accuracy, stiffness and error budget calculations for the AKDS design are presented here.

5.1.1 Background

Semiconductors have fueled economic growth in the US since their invention. Fairchild Semiconductor Corporation shares credit with Texas Instruments Incorporated for the invention and fabrication of the first integrated circuits in the late 1950's [17]. Integrated circuits are an integral component in almost every conceivable electronic device ranging from hand-held radios to satellite communication systems, computers, cell phones, video cameras and many others. The companies that design and manufacture integrated circuits owe their success in great part to the equipment that exists to test these circuits. As these circuits get faster and smaller in size, manufacturers of automated test equipment for integrated circuits face great technical challenges to create more efficient and reliable testing systems. A typical testing system for integrated circuits is shown in Figure 5.1.

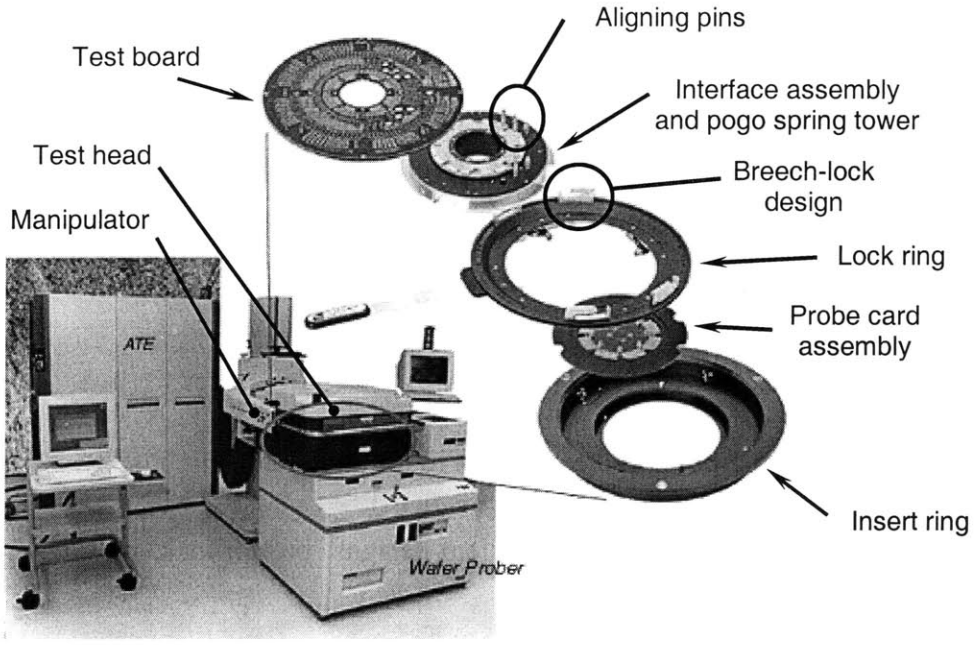

***Figure 5.1** – Semiconductor test equipment (photo courtesy of Kulicke & Soffa)*

Typically, integrated circuits are tested twice during their production cycle. They are tested once when in wafer form to single out damaged chips before packaging. They are tested again when packaged to guarantee proper function. The process of testing integrated circuits when in wafer form is called wafer probing. For wafer probing it is

necessary to establish electrical contact between the automated test machine and the integrated circuit. This is achieved with the use of several components stacked on top of each other. Referring to Figure 5.1, a test signal is produced by the test head, travels through the test board, the interface assembly (pogo spring tower plus lock ring) and the probe card until it reaches the integrated circuit. The integrated circuit processes the test signal and sends a response signal back to the test equipment. The test board and the probe card are complex printed circuit boards that spatially distribute the electric contact lines in a suitable way to test a specific integrated circuit and are thus unique to the integrated circuit under test. The pogo spring tower consists of spring loaded pins which make contact on one side with the test board and on the other side with the probe card.

The probe card utilizes a number of probes designed to make contact with specific points on the integrated circuit in wafer form. At the point of contact with the wafer, each probe is significantly thinner than a human hair. To ensure proper transmission of the signal from the test head to the wafer and back, it is important to maintain proper alignment and orientation of all the components in the system. This is achieved with the use of specialized system interfaces. The system interfaces ensure accurate and secure alignment between the test equipment and the device under test. Two common types of such interfaces include the breech-lock and pull-down block designs. The breech-lock design is shown in Figure 5.1 and the pull-down block design is shown in Figure 5.2. Both have the dual purpose of aligning the components that need to be brought in contact and applying a preload force to compress the pogo tower springs to ensure a good electrical contact. These interfaces use pin and bushing designs to align the mating components of the interface.

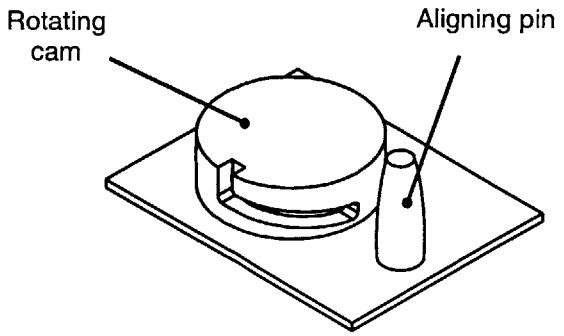

Figure 5.2 – Pull-down block design for system interface

5.1.2 The Need for Precision Fixturing

As integrated circuits get smaller in size and the alignment requirements drop from hundreds of microns (100-200μm) to a few dozens of microns (10-50μm), better alignment methods are necessary. These methods must be accurate, repeatable, reliable, cost effective and readily adaptable to existing automated test equipment.

One improvement over the typical pin and bushing alignment method was proposed by Chiu with the *Kinematic Docking System* (KDS) [18]. This system relies on exact constraint design to dock (couple) the test head to the prober head plate and replaces conventional interface designs such as breech-lock and pull-down block. This system consists of three grooves attached to the prober head plate and three balls attached to the test head forming in effect a kinematic coupling interface between the two as seen in Figure 5.3. The kinematic docking system was adapted and tested on a Teradyne AMS test head with a resulting repeatability of approximately 60μm. It is important to keep in mind that this is not the repeatability of the kinematic interface but the repeatability of the overall docking system which consists of other components as well. The repeatability achieved with the kinematic docking system was a significant improvement over other existing interfaces which have repeatability on the order of 250μm or more.

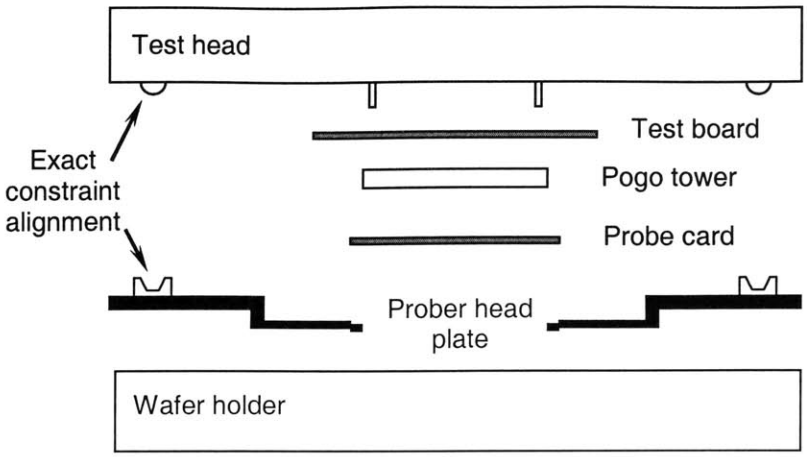

***Figure 5.3** – Kinematic docking system proposed by Chiu [18]*

The kinematic docking system incorporates other useful features that allow the ball and groove modules to latch automatically, preload the ball into the groove during docking to increase stiffness, and push the ball out of the groove during undocking. In addition to these features, the kinematic docking system can be retrofitted with motors to give it the ability to orient the test head with respect to the prober head plate in three degrees of freedom and thus compensate for parallelism errors between these two components.

5.1.3 Purpose of Case Study

The case study presented in this chapter, the *Adjustable Kinematic Docking System* (AKDS), increases the functionality of the kinematic docking system proposed by Chiu by replacing the ball and groove modules with modules from an ARKC. This results in three extra degrees of freedom which allow for active calibration of the docking system when used with a variety of test heads and prober head plates.

5.2 Design of the Adjustable Kinematic Docking System

The development of the KDS was motivated by the need to create a new interface to address several issues that existed with interfaces used at the time of its creation. One issue was the inability of existing interfaces to achieve the performance levels necessary

to support testing of integrated circuits with smaller feature sizes as demonstrated by the increasing number of interface related test problems [19]. Another issue was the uncertainty in the throughput of the testing process due to the doubtful reliability of existing interfaces.

The fundamental functional requirements for the KDS at the time of its development were:

1. Universality, meaning that the docking system could be used with different types of test heads and device handling equipment.

2. Performance, meaning that the kinematic interface of the docking system had to have a stiffness on the order of 10N/μm and contribute 25μm to the overall error budget of the system.

3. Ease of use, meaning that the proper operation of the docking system had to be intuitive.

The KDS and AKDS share the same functional requirements. The only difference between the two systems is in the implementation of the ball groove modules. For the KDS, the balls are supported through the center and mate with the grooves in a fashion similar to a conventional kinematic coupling. For the AKDS the balls are supported eccentrically. These differences are illustrated in Figure 5.4. This modification provides the AKDS with three extra degrees of freedom thus allowing it to actively compensate for planar misalignment and to be calibrated automatically. The following paragraph taken from Chiu's thesis illustrates the importance of planar misalignment compensation:

"Although the kinematic design of the docking system provides high repeatability and stability, this alone is not sufficient to provide a practical docking system. Absolute accuracy of the docking system is also required to permit proper alignment between the test head and device handler. The KDS is designed to work with any and all types of handling equipment, regardless of their design or manufacturing tolerances. Therefore, a means must be provided to adjust the relative positions of the critical interface

components in the field. Ideally, a kinematic fixture requires only six adjustments to properly align the two mating bodies. Practically, however, additional degrees of freedom are required to accommodate all types of equipment. In particular, typical test floor environments require frequent reconfiguration of test cells. Often a pool of device handlers is used with a pool of testers and therefore any tester must be able to dock to any handler. For this reason, it is desirable to allow all interfaces to be calibrated to a common standard so that interfaces do not need to be realigned before every docking cycle."

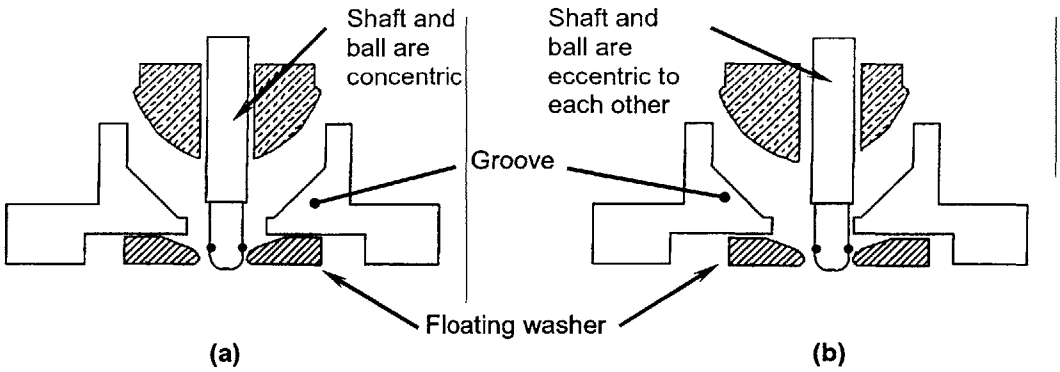

Figure 5.4 – (a) KDS and (b) AKDS

The accuracy of the KDS depends on an external calibration fixture used during its initial setup. This calibration is a manual process that requires an operator to manipulate the different components and make the necessary adjustments. This calibration operation can be performed automatically by upgrading the KDS to an AKDS resulting in decreased setup time and increased productivity.

5.3 Expected Results

This section presents theoretical results of the repeatability, accuracy and stiffness of the AKDS using the guidelines presented in the fourth chapter. It also discusses the different sources of error and quantifies the error of the AKDS.

5.3.1 Repeatability

The most sensitive direction to non-repeatability at the centroid of this design is in the plane of coupling. Neglecting the other components and assuming that the coupling is symmetrically loaded, the repeatability can be optimized from Equation (4.1) shown below as Equation (5.1) [13]. This equation gives an overestimate for the coupling repeatability (ρ) based on the groove angle (α), coefficient of friction (μ), normal stiffness at the contact points (k_{zz}) and the preload force (F). The equation is used to show how the repeatability of the design scales with design parameters. Estimates of these quantities are modeled in the paragraphs that follow:

$$\rho \approx \frac{\mu F}{18 k_{zz} \sin^2 \alpha \cos \alpha} \left(2\sqrt{3} + \cos\alpha + \sin 2\alpha\right) \tag{5.1}$$

Preload force: the preload force is expected to come primarily from the compression force required to establish a good electrical contact between the different elements in the test equipment interface. The major contribution comes from the compression pins in the pogo tower. Considering that most pogo towers have pins that require a compression force between 20-100gmf, the total force to compress a pogo tower consisting of 3000 pins ranges from 60-300kgf. This is the compression or preload force that the AKDS must be subjected to.

Coefficient of friction: the coefficient of friction can be estimated by experimentation. The coefficient of friction has to be less than the limiting coefficient of friction for the kinematic coupling to be self-centering and thus repeatable [13]. The limiting coefficient of friction depends solely on the groove geometry and ranges from 0.317 to 0.365 for a symmetric v-groove coupling whose groove angle varies between 45° and 65° [13]. A coefficient of friction below 0.1 is desirable and obtainable with the use of high pressure lubricants [12] and/or special coatings such as tungsten disulfide (WS_2) [20].

Normal stiffness at the contact points: this quantity can be estimated from Hertz contact theory according to Equations (5.2) through (5.4) [14].

$$E_e = \frac{1}{\frac{1-\nu_1^2}{E_1} + \frac{1-\nu_2^2}{E_2}} \tag{5.2}$$

$$R_e = \frac{1}{R_1^{-1} + R_2^{-1} + r_1^{-1} + r_2^{-1}} \tag{5.3}$$

$$\delta = \left(\frac{9F^2}{16 R_e E_e^2} \right)^{1/3} \tag{5.4}$$

Table 5.1 defines the parameters used in the above equations. The subscripts 1 and 2 stand for the two contacting solids (i.e. groove and ball). The normal stiffness of the contact region k_{zz} can be calculated from Equation (5.4) as the ratio of an incremental force to an incremental displacement in the direction of interest: $\Delta F / \Delta \xi$.

***Table 5.1** – Definition of the parameters to calculate the normal stiffness at the contact points*

E	Modulus of elasticity
ν	Poisson's ratio
E_e	Equivalent modulus of elasticity of the two contacting materials
R	Major radius of curvature of the contacting surfaces
r	Minor radius of curvature of the contacting surfaces
R_e	Equivalent radius of curvature of the contacting surfaces
F	Force applied to make the contact
δ	Distance of approach of two far-field points in the two solids under elastic deflection

From Equation (5.1), an overestimate for the planar repeatability of about 1.1μm is achievable under the following conditions:

- Kinematic interfaces made out of RC62 steel ($E = 204\,\text{GPa}$, $\nu = 0.29$).
- Coefficient of friction of 0.1.
- A preload of 1000N (~100kgf).
- The grooves are planar (i.e. infinite major and minor radii of curvature.
- The balls are spherical with major and minor radii of curvature of 12.7mm [0.5in].

The resulting contact stiffness k_{zz} is 65N/μm.

5.3.2 Accuracy

As discussed in section 4.1.2, the angular and linear resolution of the actuators used to control the motion of the coupling has a direct effect on the accuracy of the coupling. Recall that in-plane accuracy changes with the angular orientation of each ball and out-of-plane accuracy changes with the z coordinate of the center of each ball.

Taking (by example from Chiu's thesis) the diameter of the coupling at $1\,\text{m}\,[39.4\,\text{in}]$, the eccentricity of each ball at $6.4\,\text{mm}\,[0.25\,\text{in}]$, the angular resolution of the rotational actuators at $785\,\mu\text{rad}\,[0.045°]$ (using an angular encoder with 8000 divisions per revolution), and the linear resolution of the linear actuators at $10\,\mu\text{m}\,[3.9\times10^{-4}\,\text{in}]$, the results shown in Table 5.2 are obtained for the worst case accuracy that the AKDS can achieve as measured at the centroid of the coupling. These results were derived from Equations (2.2) and (2.3).

***Table 5.2** – Worst case accuracy in the centroid position of the AKDS*

x	y	z	θ_x	θ_y	θ_z
6.65μm	5.76μm	10μm	26.7μrad	23.1μrad	9.97μrad

The eccentricity of the balls is an important parameter in the design of the ARKC and AKDS. A larger eccentricity results in a larger working volume but also in decreased resolution. For the AKDS, the eccentricity was chosen to achieve planar displacements of

$\pm 4.3\,\text{mm}[\pm 0.170\,\text{in}]$ in the x direction, $\pm 7.4\,\text{mm}[\pm 0.290\,\text{in}]$ in the y direction and $\pm 1.3\times 10^{-2}\,\text{rad}\,[\pm 0.7°]$ in θ_z . These displacements are enough to accommodate positional deviations from nominal in the different components that need to be coupled together (i.e. test head with prober head plate).

5.3.3 Stiffness

Equation (5.5) shows the global stiffness matrix of a standard v-groove kinematic coupling [13]. The global stiffness matrix is a diagonal matrix when the centroid of the coupling lies in the plane of the contact points. Equation (5.5) can be obtained by following the procedure outlined in section 4.1.3.

$$K_g = k_{zz} \cdot \begin{bmatrix} 3\sin^2\alpha & 0 & 0 & 0 & 0 & 0 \\ 0 & 3\sin^2\alpha & 0 & 0 & 0 & 0 \\ 0 & 0 & 6\cos^2\alpha & 0 & 0 & 0 \\ 0 & 0 & 0 & 3R_k^2\cos^2\alpha & 0 & 0 \\ 0 & 0 & 0 & 0 & 3R_k^2\cos^2\alpha & 0 \\ 0 & 0 & 0 & 0 & 0 & 6R_k^2\sin^2\alpha \end{bmatrix} \tag{5.5}$$

In the above expression, k_{zz} stands for the normal stiffness at the contact points (calculated from Hertz theory), α stands for the groove angle (Figure 4.1) and R_k is the distance from the centroid of the coupling to each point of contact. The stiffness matrix contains information about the force-deflection behavior of the coupling as seen from the centroid.

The contact stiffness is calculated at $k_{zz} = 65\,\text{N}/\mu\text{m}$ using the values of section 5.3.1. Choosing $\alpha = 58°$ to obtain optimal repeatability (see section 4.1.1) and $R_k = 0.5\,\text{m}$, the following results are obtained for a coupling preloaded with 1000N:

- A lateral force of 200N in the x direction displaces the centroid of the coupling by 1.4μm in the same direction. The same result is obtained for the y direction.
- A vertical force of 200N in the z direction displaces the centroid by 1.8μm.

- A torque of 100N·m in the direction of θ_x or θ_y rotates the centroid of the coupling by 7.3μrad in the same direction.
- A torque of 100N·m in the direction of θ_z rotates the centroid of the coupling by 1.4μrad in that direction.

These disturbance forces and torques result from variations as high as 20% in the preload force. It is unlikely to see variations from nominal of this magnitude, hence the results of the theory should be taken as very conservative estimates (i.e. by about a factor of 4).

5.3.4 Sources of Error

There are several sources of error for the ARKC. A discussion of these errors and how they can be quantified is found in the previous chapter. The sensitivity of the coupling to each error depends on the configuration and orientation of the balls. The values shown in Table 5.3 correspond to worst case errors that can be expected from the AKDS. The last row shows the total error in each direction. This total is an overestimate because it simply adds the errors without taking into account statistical variations and possible cancellations between them. The total error in each direction must be modeled statistically to get a more reasonable estimate. Statistical modeling techniques to quantify these errors are a current topic of research.

***Table 5.3** – Quantification of several types of errors that enter the error budget of the AKDS*

Type of error	x [μm]	y [μm]	z [μm]	θ_x [μrad]	θ_y [μrad]	θ_z [μrad]
Machining tolerances	±17	±15	±0	±0	±0	±25
Contact deformation	±0.56	±0.56	±0.60	±0.002	±0.11	±0.009
Bearing runout	±5	±5	±0	±0	±0	±10
Actuator error	±1.33	±1.15	±2.00	±5.33	±4.6	±2.00
Total	**±23.9**	**±21.7**	**±2.6**	**±5.3**	**±4.7**	±37

For machining tolerances, it was assumed that the eccentricity of the axis of rotation of each ball of the AKDS was 6.3×10^{-3} m [0.25 in] and that the tolerance on this eccentricity was $\pm12.7\,\mu$m [$\pm 5\times10^{-4}$ in]. For contact deformation, it was assumed that the coupling was preloaded with 1000N and that a reversing load of 150N in x, y and z was applied at the centroid of the coupling. The bearing runout was assumed at 5μm. Both angular and linear actuators were assumed to have ± 20% error in their positioning resolution which in the present case translates to an angular error of ±157μrad and a linear error of ±2μm.

5.3.5 Conclusions on Prototype Performance

These results indicate that the AKDS has the capability to meet the performance requirements for next generation test equipment (i.e. alignment better than 50μm and 50μrad) but special attention needs to be put into minimizing the errors that enter the error budget. These errors are large compared to the accuracy of the coupling. Machining tolerances are the main source of error affecting the in-plane performance of the AKDS while the actuators are the main source of error affecting out-of-plane performance. Fortunately, both errors can be mapped, meaning that they can be eliminated by implementing closed-loop control.

Chapter 6

SUMMARY AND FUTURE WORK

6.1 Summary

A positioning device that can be used as a precision coupling/fixture in automated manufacturing operations was developed. The device, called the adjustable and repeatable kinematic coupling (ARKC), is based on a three groove kinematic coupling. The kinematic fixture achieves motion in six degrees of freedom with great accuracy and repeatability.

This thesis compliments Rodríguez's experimental work [2] and contributes the following:

1. **Verification of the mathematical model for adjustable kinematics:** the motion of the centroid of the coupling is modeled according to Equations (2.2) and (2.3). This model is used in the fourth chapter to quantify the performance of the ARKC (i.e. its repeatability, accuracy and stiffness). The model is verified experimentally via a prototype ARKC tested in the laboratory. The results show that the motion of the coupling agrees with the theoretical predictions with less than 13% error. This error is largely systematic and will be mapped and removed from the system at a later date.

2. **The error budget analysis of the coupling:** the error budget is examined in detail in the fourth chapter. This analysis tool is valuable to guarantee that the ARKC meets its

performance requirements. Some errors considered in the error budget are: errors due to manufacturing tolerances, errors due to bearing runout, errors due to contact deformations at the kinematic interfaces of the coupling, and errors due to the actuators. The error budget shows that errors in the location of the axis of rotation of each ball have the most significant effect on the accuracy of the coupling. These errors include those due to manufacturing tolerances and bearing runout. The errors due to manufacturing tolerances are systematic and can be measured and corrected via control. The errors due to bearing runout are random and cannot be corrected. The analysis shows that the performance of the coupling can compare favorably with more expensive, robotic fixtures. The performance of the coupling will be improved during subsequent work/optimization on the design of the ARKC prototype.

3. **A discussion about the implementation of the ARKC in flexible manufacturing systems:** The third chapter examines a flexible manufacturing scenario that makes use of the ARKC. The implementation of the coupling is described in detail to highlight the ways in which it increases productivity by reducing production time. Two industrial communication networks (DeviceNet and Foundation Fieldbus) enable the seamless integration of the ARKC into modern automated manufacturing systems. These communication networks are discussed emphasizing the ways in which they increase the functionality of the ARKC, allowing it to be seamlessly integrated into automated manufacturing processes.

4. **A case study that illustrates the use of the ARKC concept in automated testing of integrated circuits:**

The case study examined in the thesis proposes the modification of an existing kinematic docking system (KDS) for mating and aligning components in automated test equipment for integrated circuits. This modification increases the functionality of the kinematic docking system by enabling its automated setup and calibration. The modified docking system, called the adjustable kinematic docking system (AKDS), was studied to determine whether it could meet the performance requirements of next generation test equipment. The results shown in Table 5.2 and Table 5.3 correspond to the positioning

accuracy of the AKDS and the maximum error expected in each direction respectively. These results are summarized in Table 6.1 below.

***Table 6.1** – AKDS performance summary*

Direction	x	y	z	θ_x	θ_y	θ_z
Accuracy (i.e. worst-case resolution)	6.6μm	5.8μm	10μm	27μrad	23μrad	10μrad
Worst-case systematic error	± 18.9μm	± 16.7μm	± 2.6μm	± 5μrad	± 5μrad	± 27μrad
Random error	± 5μm	± 5μm	± 0μm	± 0μrad	± 0μrad	± 10μrad

These results indicate that the AKDS has the capability to meet the performance requirements for next generation test equipment (i.e. alignment better than 50μm and 50μrad) but special attention needs to be put into minimizing the errors that enter the error budget. These errors are large compared to the accuracy of the coupling. Machining tolerances are the main source of error affecting the in-plane performance of the AKDS while the actuators are the main source of error affecting out-of-plane performance. Fortunately, both errors can be mapped, meaning that they can be eliminated by implementing closed-loop control.

The results discussed above for the performance of the AKDS are theoretical. Verification of these results against hardware is the subject of future research. As a preliminary step toward this verification, a prototype ARKC was constructed and tested in the laboratory. This prototype ARKC used dual motion stepper motors to move each ball via open loop control. The data obtained from the tests shows that theoretical and experimental results agree with less than 13% error. Again, this error will be minimized through future mapping/work on the coupling.

6.2 Topics for Future Research

There is an immediate question that emerges from the writing of this thesis. How do the errors in the error budget add together? The results presented in Table 6.1 assume that all errors are added. This is not likely the case because some errors may cancel each other. In this sense, the error budget presented in this thesis is a conservative overestimate. Since these errors affect the design of the coupling in a significant way, it is important to obtain more accurate estimates of their magnitude and their effect on performance. One modeling approach proposed by Barraja and Vallance uses multivariate error analysis to allocate tolerances to dimensions in kinematic couplings in order to reduce manufacturing cost [5]. The PSDAM lab at MIT is also conducting research in this area in order to better understand these errors using statistical modeling techniques. Subsequent work on reducing random errors and improving the calibration of the coupling is planned.

REFERENCES

[1] Culpepper, M. L. "Design and Application of Compliant Quasi-Kinematic Couplings," Ph.D. thesis, M.I.T., Cambridge, MA, 2000.

[2] Rodríguez, M. E. "Design and Manufacturing of and ARKC (Adjustable and Repeatable Kinematic Coupling)," B.S. thesis, M.I.T., Cambridge, MA, 2002.

[3] Culpepper, M. L., Araque C. A. and Rodríguez, M. E. "Design of accurate and repeatable kinematic couplings," ASPE Annual Meeting article, Fall 2002 (not yet published).

[4] Boyes, W. E., Ed., *Handbook of Jig and Fixture Design*. Society of Manufacturing Engineers (SME), Dearborn, MI, 1989, pp. 2-24 – 2-25.

[5] Barraja, M. and Vallance, R., "Tolerance allocation for kinematic couplings," Precision Systems Laboratory, University of Kentucky, Lexington, KY, (not yet published).

[6] Taylor, J. B. and Tu, J. F., "Precision X-Y microstage with maneuverable kinematic coupling mechanism," *Precision Engineering*, vol. 18, no. 2/3, April/May, pp. 85-94, 1996.

[7] Kalpakjian, S. and Schmid, S. R., *Manufacturing Engineering and Technology*. Prentice-Hall, Upper Saddle River, NJ, 4th edition, 2001, pp. 1023-1024.

[8] Rembold, U., Nnaji B.O. and Storr A., *Computer Integrated Manufacturing and Engineering*. Addison-Wesley, 1993.

[9] DeviceNet is managed by the Open DeviceNet Vendor Association (ODVA): http://www.odva.org.

[10] Foundation Fieldbus is managed by the Fieldbus Foundation: http://www.fieldbus.org.

[11] Olexa, R., senior ed, "Flexibility in assembly equipment," *Manufacturing Engineering*, vol. 128, no. 3, p. 65, 2002.

[12] Slocum, A. H. and Donmez, A., "Kinematic couplings for precision fixturing – part 2: experimental determination of repeatability and stiffness," *Precision Engineering*, vol. 10, no. 3, pp. 115-121, 1988.

[13] Hale, L. C. and Slocum, A. H., "Optimal design techniques for kinematic couplings," *Precision Engineering*, vol. 25, no. 2, pp. 114-127, 2001.

[14] Johnson, K. L., *Contact Mechanics*. Cambridge University Press, 1996, pp. 84-106.

[15] Hale, L. C., "Principles and techniques for designing precision machines," Ph.D. thesis, M.I.T., Cambridge, MA, 1999.

[16] Slocum, A. H., "Design of three groove kinematic couplings," *Precision Engineering*, vol. 14, no. 2, pp. 67-76, 1992.

[17] "Fairchild Semiconductor Corporation" *Encyclopaedia Britannica* <http://search.eb.com/eb/article?eu=138478> [accessed July 4, 2002]

[18] Chiu, M. A., "Roadmap of mechanical systems design for the semiconductor automatic test equipment industry," Ph.D. thesis, M.I.T., Cambridge, MA, 1998.

[19] Chiu, M. A., Godfrey, J. and Tivnan, J., "Characterizing the Teradyne A50/KLA 1201 test cell," In *Teradyne Users Group Proceedings*, 1996.

[20] Telephone conversation with Ken Klapper from Brycoat, Inc.

Appendix A

ADJUSTABLE KINEMATIC MODEL OF THE ARKC

A.1 In-Plane Motion

In-plane motion of the ARKC (i.e. motion in x, y and θ_z) is modeled according to Figure A.1.

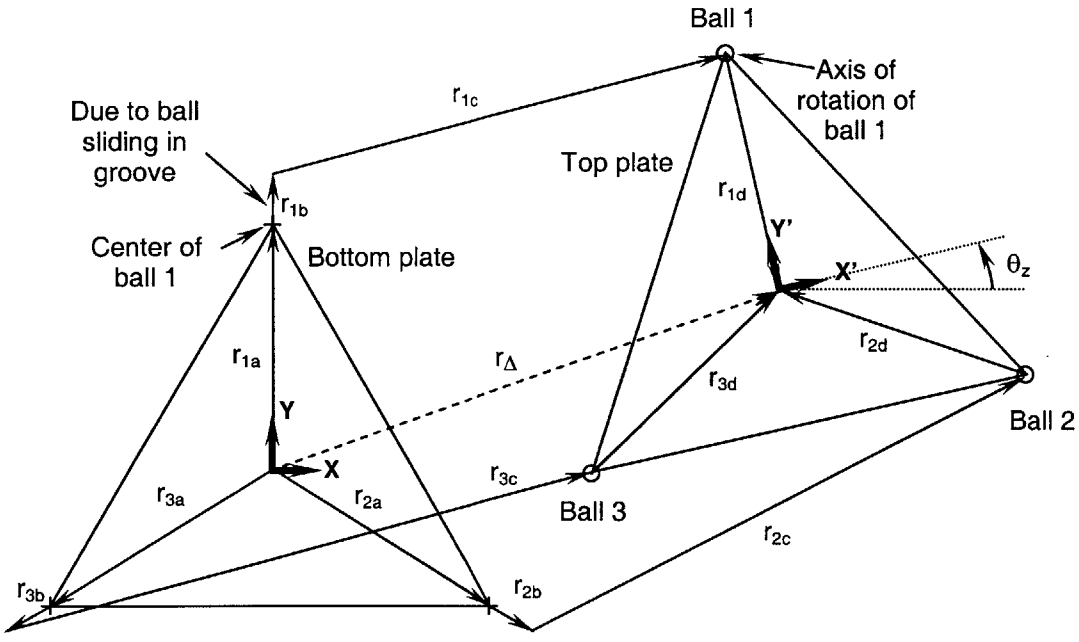

***Figure A.1** – Vector loop model for in-plane motion of the ARKC*

Figure A.1 shows three vector loops:

$$\begin{aligned}&\vec{r}_{1a}+\vec{r}_{1b}+\vec{r}_{1c}+\vec{r}_{1d}=\vec{r}_{\Delta}\\&L_{1a}\left(\cos(\theta_{1a})\cdot\hat{i}+\sin(\theta_{1a})\cdot\hat{j}\right)+L_{1b}\left(\cos(\theta_{1b})\cdot\hat{i}+\sin(\theta_{1b})\cdot\hat{j}\right)\\&+L_{1c}\left(\cos(\theta_{1c})\cdot\hat{i}+\sin(\theta_{1c})\cdot\hat{j}\right)+L_{1d}\left(\cos(\theta_{1d})\cdot\hat{i}+\sin(\theta_{1d})\cdot\hat{j}\right)=x\cdot\hat{i}+y\cdot\hat{j}\end{aligned}\tag{A.1}$$

$$\begin{aligned}&\vec{r}_{2a}+\vec{r}_{2b}+\vec{r}_{2c}+\vec{r}_{2d}=\vec{r}_{\Delta}\\&L_{2a}\left(\cos(\theta_{2a})\cdot\hat{i}+\sin(\theta_{2a})\cdot\hat{j}\right)+L_{2b}\left(\cos(\theta_{2b})\cdot\hat{i}+\sin(\theta_{2b})\cdot\hat{j}\right)\\&+L_{2c}\left(\cos(\theta_{2c})\cdot\hat{i}+\sin(\theta_{2c})\cdot\hat{j}\right)+L_{2d}\left(\cos(\theta_{2d})\cdot\hat{i}+\sin(\theta_{2d})\cdot\hat{j}\right)=x\cdot\hat{i}+y\cdot\hat{j}\end{aligned}\tag{A.2}$$

$$\begin{aligned}&\vec{r}_{3a}+\vec{r}_{3b}+\vec{r}_{3c}+\vec{r}_{3d}=\vec{r}_{\Delta}\\&L_{3a}\left(\cos(\theta_{3a})\cdot\hat{i}+\sin(\theta_{3a})\cdot\hat{j}\right)+L_{3b}\left(\cos(\theta_{3b})\cdot\hat{i}+\sin(\theta_{3b})\cdot\hat{j}\right)\\&+L_{3c}\left(\cos(\theta_{3c})\cdot\hat{i}+\sin(\theta_{3c})\cdot\hat{j}\right)+L_{3d}\left(\cos(\theta_{3d})\cdot\hat{i}+\sin(\theta_{3d})\cdot\hat{j}\right)=x\cdot\hat{i}+y\cdot\hat{j}\end{aligned}\tag{A.3}$$

Note that $\theta_{id}=\theta_{ia}+\pi+\theta_z$ where the subscript $i=1,2,3$ stands for each vector loop. Substituting this expression into Equations (A.1) through (A.3) we obtain Equations (A.4) and (A.5).

$$L_{ia}\cos(\theta_{ia})+L_{ib}\cos(\theta_{ib})+L_{ic}\cos(\theta_{ic})+L_{id}\cos(\theta_{ia}+\pi+\theta_z)-x=0\tag{A.4}$$

$$L_{ia}\sin(\theta_{ia})+L_{ib}\sin(\theta_{ib})+L_{ic}\sin(\theta_{ic})+L_{id}\sin(\theta_{ia}+\pi+\theta_z)-y=0\tag{A.5}$$

Using the trigonometric identities $\cos(\alpha+\beta)=\cos\alpha\cos\beta-\sin\alpha\sin\beta$ and $\sin(\alpha+\beta)=\sin\alpha\cos\beta-\cos\alpha\sin\beta$ and the small angle approximations $\sin(\theta_z)\approx\theta_z$ and $\cos(\theta_z)\approx 1$, we obtain

$$\begin{aligned}\cos(\theta_{ia}+\pi+\theta_z) &= \cos(\theta_{ia}+\pi)\cos(\theta_z)-\sin(\theta_{ia}+\pi)\sin(\theta_z)\\ &= \sin(\theta_{ia})\sin(\theta_z)-\cos(\theta_{ia})\cos(\theta_z)\\ &= \theta_z\sin(\theta_{ia})-\cos(\theta_{ia})\end{aligned} \tag{A.6}$$

$$\begin{aligned}\sin(\theta_{ia}+\pi+\theta_z) &= \sin(\theta_{ia}+\pi)\cos(\theta_z)+\cos(\theta_{ia}+\pi)\sin(\theta_z)\\ &= -\sin(\theta_{ia})\cos(\theta_z)-\cos(\theta_{ia})\sin(\theta_z)\\ &= \sin(\theta_{ia})-\theta_z\cos(\theta_{ia})\end{aligned} \tag{A.7}$$

Substituting Equations (A.6) and (A.7) into Equations (A.4) and (A.5), and writing in matrix form yields the final result shown in Equation (A.8),

$$\begin{bmatrix} C[\theta_{1b}] & 0 & 0 & -1 & 0 & L_{1d}\,S[\theta_{1a}] \\ S[\theta_{1b}] & 0 & 0 & 0 & -1 & -L_{1d}\,C[\theta_{1a}] \\ 0 & C[\theta_{2b}] & 0 & -1 & 0 & L_{2d}\,S[\theta_{2a}] \\ 0 & S[\theta_{2b}] & 0 & 0 & -1 & -L_{2d}\,C[\theta_{2a}] \\ 0 & 0 & C[\theta_{3b}] & -1 & 0 & L_{3d}\,S[\theta_{3a}] \\ 0 & 0 & S[\theta_{3b}] & 0 & -1 & -L_{3d}\,C[\theta_{3a}] \end{bmatrix} \cdot \begin{pmatrix} L_{1b} \\ L_{2b} \\ L_{3b} \\ x \\ y \\ \theta_z \end{pmatrix} = \begin{pmatrix} (L_{1d}-L_{1a})C[\theta_{1a}]-L_{1c}\,C[\theta_{1c}] \\ (L_{1d}-L_{1a})S[\theta_{1a}]-L_{1c}\,S[\theta_{1c}] \\ (L_{2d}-L_{2a})C[\theta_{2a}]-L_{2c}\,C[\theta_{2c}] \\ (L_{2d}-L_{2a})S[\theta_{2a}]-L_{2c}S[\theta_{2c}] \\ (L_{3d}-L_{3a})C[\theta_{3a}]-L_{3c}\,C[\theta_{3c}] \\ (L_{3d}-L_{3a})S[\theta_{3a}]-L_{3c}\,S[\theta_{3c}] \end{pmatrix} \tag{A.8}$$

where **C[θ]** and **S[θ]** stand for cosine and sine respectively.

A.2 Out-of-Plane Motion

Out-of-plane motion of the ARKC (i.e. motion in z, θ_x and θ_y) can be analyzed with the help of analytic geometry and vector algebra. The centers of the balls of the ARKC define a plane. Any normal vector to this plane contains information about the orientation of the plane. Let $B_1=(x_1,y_1,z_1)$, $B_2=(x_2,y_2,z_2)$ and $B_3=(x_3,y_3,z_3)$ be the centers of balls 1, 2 and 3 respectively. We can define two vectors between these points as follows:

$$\vec{V}_{12} = (x_2 - x_1)\cdot\hat{i} + (y_2 - y_1)\cdot\hat{j} + (z_2 - z_1)\cdot\hat{k} \tag{A.9}$$

$$\vec{V}_{13} = (x_3 - x_1)\cdot\hat{i} + (y_3 - y_1)\cdot\hat{j} + (z_3 - z_1)\cdot\hat{k} \tag{A.10}$$

These vectors lie in the plane defined by the three ball centers and their cross product defines a normal vector to this plane.

$$\begin{aligned}\vec{N} = \vec{V}_{13}\times\vec{V}_{12} = &[(y_2 - y_1)(z_3 - z_1) - (z_2 - z_1)(y_3 - y_1)]\cdot\hat{i} \\ &[(z_2 - z_1)(x_3 - x_1) - (x_2 - x_1)(z_3 - z_1)]\cdot\hat{j} \\ &[(x_2 - x_1)(y_3 - y_1) - (x_3 - x_1)(y_2 - y_1)]\cdot\hat{k}\end{aligned} \tag{A.11}$$

The orientation of the plane (i.e. θ_x and θ_y) is obtained from the components of this normal vector:

$$\theta_x \approx \mathbf{tan}(\theta_x) = -\frac{\hat{N}\cdot\hat{j}}{\hat{N}\cdot\hat{k}} = -\frac{(z_2 - z_1)(x_3 - x_1) - (x_2 - x_1)(z_3 - z_1)}{(x_2 - x_1)(y_3 - y_1) - (x_3 - x_1)(y_2 - y_1)} \tag{A.12}$$

$$\theta_y \approx \mathbf{tan}(\theta_y) = \frac{\hat{N}\cdot\hat{i}}{\hat{N}\cdot\hat{k}} = \frac{(y_2 - y_1)(z_3 - z_1) - (z_2 - z_1)(y_3 - y_1)}{(x_2 - x_1)(y_3 - y_1) - (x_3 - x_1)(y_2 - y_1)} \tag{A.13}$$

Equations (A.12) and (A.13) become Equations (A.14) and (A.15) below after substituting the values for x_i and y_i:

$$\theta_x \approx -\frac{L_{1d}\cdot(s[\theta_{1a}]\cdot\theta_z - c[\theta_{1a}])\cdot(z_2 - z_3) + L_{2d}\cdot(s[\theta_{2a}]\cdot\theta_z - c[\theta_{2a}])\cdot(z_3 - z_1) + L_{3d}\cdot(s[\theta_{3a}]\cdot\theta_z - c[\theta_{3a}])\cdot(z_1 - z_2)}{L_{1d}\cdot L_{2d}\cdot s[\theta_{2a} - \theta_{1a}] + L_{2d}\cdot L_{3d}\cdot s[\theta_{3a} - \theta_{2a}] + L_{3d}\cdot L_{1d}\cdot s[\theta_{1a} - \theta_{3a}]} \tag{A.14}$$

$$\theta_y \approx \frac{L_{1d}\cdot(s[\theta_{1a}] + c[\theta_{1a}]\cdot\theta_z)\cdot(z_2 - z_3) + L_{2d}\cdot(s[\theta_{2a}] + c[\theta_{2a}]\cdot\theta_z)\cdot(z_3 - z_1) + L_{3d}\cdot(s[\theta_{3a}] + c[\theta_{3a}]\cdot\theta_z)\cdot(z_1 - z_2)}{L_{1d}\cdot L_{2d}\cdot s[\theta_{2a} - \theta_{1a}] + L_{2d}\cdot L_{3d}\cdot s[\theta_{3a} - \theta_{2a}] + L_{3d}\cdot L_{1d}\cdot s[\theta_{1a} - \theta_{3a}]} \tag{A.15}$$

Where the approximations $\theta_x \approx \tan(\theta_x)$ and $\theta_y \approx \tan(\theta_y)$ were used. These approximations are valid because the motion of the ARKC involves only small rotations (i.e. less than 5°) in these directions.

The position of the centroid of the triangle formed by the ball centers (i.e. the centroid of the coupling) is given by Equation (A.16).

$$z_c \approx L_{1d} \cdot (\theta_y \cdot c[\theta_{1a}] - \theta_x \cdot s[\theta_{1a}]) + z_1 \tag{A.16}$$